Karlsruher Institut für Technologie

Emulation of the One-Dimensional Fermi-Hubbard Model Using Superconducting Qubits

Emulation des eindimensionalen Fermi-Hubbard-Models unter Verwendung von supraleitenden Qubits

Masterarbeit
von

Jan-Michael Reiner

am Institut für Theoretische Festkörperphysik
der Fakultät für Physik

Erstgutachter:	Prof. Gerd Schön
Zweitgutachter:	Prof. Alexey Ustinov
Betreuender Mitarbeiter:	Dr. Michael Marthaler

12. Mai 2015

Eigenständigkeitserklärung

Ich versichere wahrheitsgemäß, die Arbeit selbstständig angefertigt, alle benutzten Hilfsmittel vollständig und genau angegeben und alles kenntlich gemacht zu haben, was aus Arbeiten anderer unverändert oder mit Abänderungen entnommen wurde.

Karlsruhe, 12. Mai 2015, ...

(**Jan-Michael Reiner**)

Contents

Chapter 1

Introduction

Classical computers consistently improved in the past and continue to do so at a stable rate, such that even personal computers or a modern smartphone have become amazingly powerful devices. Yet there are countless computational problems that cannot be solved in a sufficiently small amount of time. A famous example is the factorization of large prime numbers. The computation time increases exponentially with the size of the prime number; at least a faster algorithm has not been found yet. Shor's algorithm [1] on the other hand shows that this problem can be solved in polynomial time using a quantum computer, which has been demonstrated on a small scale in experiment [2]. Another challenge for classical computers is the simulation of quantum systems. In general the Hilbert space of a quantum system scales exponentially with the number particles and states, due to the number of possible configurations to excite these states. While a classical computer cannot treat this problem efficiently, a quantum computer can [3].

Using quantum devices to address such computational problems was proposed by Richard Feynman in 1982 [4], and has since been intensively studied. However the estimated amount of physical quantum bits (qubits) needed for the realization of a universal quantum computer with implemented quantum error correction is upwards of ten thousand [5] for the realization of one logical qubit. Therefore a universal quantum computer consisting of a large number of logical qubits would demand a very large number of physical qubits. However, the state of technology is still at the level of the implementation of a few qubits with the focus on improving the properties of single qubits.

An approach besides universal quantum computing is quantum emulation. Instead of a multi-purpose device that allows for the simulation of an arbitrary problem, a quantum emulator is a quantum device that emulates one specific problem; an analogue quantum emulator is an artificial quantum device with a Hamiltonian which is equivalent to the Hamiltonian of a quantum system it emulates. Such a device potentially requires far less qubits to function than a multi-purpose quantum computer.

Systems of great interest for emulation are fermionic systems. These systems are of course very important in nature, but for larger system sizes, they are often not treatable

trough analytic calculation or numerical simulation with a classical computer.

An example of an interesting fermionic model is the Fermi-Hubbard model. Emulators of this model based on atoms in optical traps have been realized [6, 7], but the manipulation and readout of single atoms in these systems is difficult. The technology this thesis focuses on are superconducting circuits: As macroscopic structures, they potentially allow for easy manipulation and scalability [8, 9]. There are also several designs to implement a qubit in a superconducting circuit [10, 8], where we focus on the transmon qubit [11]. Modern transmons designs already have relatively high coherence times [12, 13], which in turn may lead to relatively long emulation times. The idea is to represent fermionic states—which can be occupied or non-occupied—by qubits as two level systems. This is however nontrivial: Qubit excitations are bosonic with different commutation relations than fermions; the emulators based on optical traps simply use fermions as particles in the trap. Fortunately, there are solutions to correctly map fermions onto qubits.

This thesis will construct a circuit design for an emulator for the one-dimensional Fermi-Hubbard model using transmon qubits in a superconducting circuit.

We will start by explaining the concept of quantum emulation in more detail and give requirements an emulator needs to fulfill. We continue by giving an overview how quantum circuits are treated in calculations and how the tunable transmon qubit as the fundamental element of the emulator circuit functions. We explain the Jordan-Wigner transformation and apply it to the one-dimensional Fermi-Hubbard model to see its equivalence to a qubit system, where the qubits are coupled by their σ^z and σ^x Pauli operators.

We will proceed by giving circuit diagrams that produce these types of couplings between tunable transmons. We will show that the σ^x-type interaction can be achieved by coupling the transmons through additional inductances or capacitances, and explain why the method of using capacitances is preferable. We will also derive how the coupling of the tunable transmons by a mutual inductance formed by their intrinsic inductances will couple the qubits by their σ^z operators, which has not been proposed before. This is followed by the full circuit diagram for the emulator of the Fermi-Hubbard model and a discussion about the tunability of its parameters as well as the experimental realization in possibly near future.

Subsequently, we will explain the standard initialization scheme for a transmon in detail. In addition to the usual readout procedure, we will also provide a readout method based on the mechanism of coupling to a tunable transmon via a mutual inductance. This is followed by a discussion how to treat the situation of multiple qubits coupled to each other, as this is the situation in the emulator and will enable us to initiate a certain quantum state in the emulator and measure the emulation result afterwards.

In the end, we will briefly address certain sources of error in the emulator, which is especially important, since there are no error correcting methods implemented in the emulator. We will focus on general sources of error like temperature and disorder, but also specific problems of our emulator concerning the level spectrum of a transmon. This

is why we will also show an approach to gain confidence in the emulation results, before we will eventually draw a conclusion of the findings of this thesis.

Chapter 2

Elementary Concepts

In this chapter, we start by explaining what quantum emulation and the general idea behind it is. We then explore the technology which we intend to use to build a quantum emulator, namely superconducting circuits. For this we also introduce tunable transmons as a key element of the circuits in mind. We proceed by establishing how these quantum circuits will help us to emulate fermionic systems and we will explicitly conceptualize the design of an emulator for the Fermi-Hubbard model in one dimension.

This will give us the foundation to address the concrete circuit design of our quantum emulator, its range of validity and limitations, as well as the discussion of certain error sources in the following chapters.

2.1 Quantum Emulation

Let us explore the concept of quantum emulation in more detail. Imagine a problem one wants to find the solution for, but there is no (practical) analytic solution to it, and the problem is also inefficient to simulate numerically on a classical computer. This is for example the case for the time evolution of fermionic systems with a number of n different fermionic states; without demanding any sorts of restrictions, the computation time on a classical computer would generally scale exponentially, since the problem can always be broken down to the diagonalization of a $2^n \times 2^n$ matrix. For this reason large values of n are not accessible.

On a universal quantum computer this specific problem would only scale polynomially in the number of qubits and operations [3], but the realization of such a device is in quite distant future. The difficulty here is the number of quantum bits one has to implement in hardware to account for one logical qubit, which is still estimated to be in the ten thousands, if one implements quantum error correction [5]. A multi-purpose quantum computer consisting out of a large number of logical qubits would therefore need an even larger amount of physical qubits to be implemented on the hardware level. However, the current status of the technology is rather to have single or a few qubits on a chip and the focus is still on improving the properties of individual quantum bits.

A question that arises now, is what useful applications are there in between the state of having single qubits on a chip and implementing millions for a universal quantum computer. This is where the concept of quantum emulation comes in. An emulator captures the features of a given system and emulates—or imitates—them on a different technological system. In quantum emulation, one seeks to obtain information about quantities or the time evolution of a specific quantum system (which cannot be determined through calculation or measurement) by creating an artificial quantum system which is equivalent to the original one, one is interested in; meaning their Hamiltonians are equivalent. The artificial system—the quantum emulator—is designed such that desired initial conditions can be set and manipulated, and the quantities one wants to study are accessible through measurement.

The anticipated benefit is obvious: Due to only emulating a specific system instead of potentially simulating any given system, the quantum emulator should need significantly less qubits than a multi-purpose quantum computer. The goal of this thesis is to conceptualize an emulator that would work with an amount of qubits to build it in near future, yet does not produce trivial results. To limit the number of qubits we avoid digital information processing and logic gates, and focus instead on an analog approach, where our quantum emulator intrinsically has the desired Hamiltonian.

The cue about nontrivial results brings us to a final concern: addressing what a quantum emulator should accomplish. This was nicely evaluated and then specified by Hauke et al. in four criteria [14]:

1. Relevance: The emulated systems should be of some relevance for applications or our understanding.

2. Controllability: A quantum emulator should allow for broad control of the parameters of the emulated system, and for control of preparation, initialization, manipulation, evolution, and detection of the relevant observables of the system.

3. Reliability: Within some prescribed error, one should be assured that the observed physics of the quantum emulator corresponds faithfully to that of the ideal model whose properties we seek to understand.

4. Efficiency: The quantum emulator should solve problems more efficiently than it is practically possible on a classical computer.

After we will have established our design of a quantum emulator, we will have to examine, whether it holds up against these four conditions. But first we need to develop the concepts necessary to design the emulator.

2.2 Superconducting Circuits

The question at this point is of course what technology to use to build a quantum emulator. There are multiple options of artificial and controllable quantum systems, an

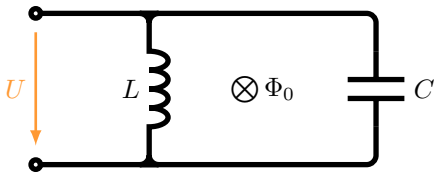

Figure 2.1: Circuit diagram of an LC circuit with inductance L and capacitance C, with a voltage U across the elements. An external magnetic flux Φ_0 is passing through the loop.

example would be ultra cold gases in optical traps. This thesis will work with superconducting circuits, as they offer good capabilities for external manipulation and are potentially easily scalable towards larger systems [8, 9]. Therefore, they are a promising candidate for a realization of a quantum emulator in the foreseeable future.

This section will now build the foundation of how to treat such circuits and their quantum mechanical nature by introducing methods to calculate the behavior of any given circuit, which will be used throughout this document. Also introduced will be the transmon qubit as the fundamental element of our emulator design.

2.2.1 Treating Quantum Circuits

Basically, there are three different electric components to wire together in a superconducting circuit. Because of the superconductivity, dissipation through resistors can be ignored. However, a piece or loop of wire will intrinsically obtain a certain inductance, and wires placed next to each other will form a capacitance. A third and very important element is the Josephson junction. Such a junction is formed by two superconductors connected through a very small isolating layer functioning as a weak link between them; in superconducting circuits the size of these layers is typically of the order of nanometers. They can be produced by applying superconducting metal on a substrate, letting it build up a thin layer of oxide and then applying superconducting metal on top [10]. The nonlinear effect these junctions produce is crucial to the functionality of our circuits, which will be seen in the application in the transmon qubit.

To perform calculations on the various circuits in the latter quickly, we will always use the same procedure. To understand where it stems from, let us first derive it by the simple example of an LC circuit shown in figure 2.1, which means a loop with a capacitance C, an inductance L, a voltage U across those elements and a constant external flux Φ_0 through the loop. The current through C can be expressed as the time derivative of its charge $\dot{Q} = C\dot{U}$, for current I_L through the inductance it holds that $\dot{I}_L = -\frac{1}{L}U$. By also regarding that voltage can be written as time derivative of induced magnetic flux, hence $U = \dot{\Phi}$, and using Kirchhoff's law for currents we find

$$0 = C\dot{U} + \frac{1}{L}\int U \,\mathrm{d}t = C\ddot{\Phi} + \frac{1}{L}(\Phi - \Phi_0), \tag{2.1}$$

where Φ_0 enters as the constant of integration; the reason for that will be clear in a

second. This result can be compared with the Euler-Lagrange equation $0 = \frac{\mathrm{d}}{\mathrm{d}t}\frac{\partial \mathcal{L}}{\partial \dot{\Phi}} - \frac{\partial \mathcal{L}}{\partial \phi}$, leading to a Lagrangian

$$\mathcal{L}_{\mathrm{LC}}(\dot{\Phi}, \Phi) = \frac{1}{2}C\dot{\Phi}^2 - \frac{1}{2L}(\Phi - \Phi_0)^2. \tag{2.2}$$

We can now see how the capacitor contributes a kinetic energy term $T_C = \frac{1}{2}C\dot{\Phi}^2$ and the inductance a potential energy $V_L = \frac{1}{2L}(\Phi - \Phi_0)^2$, where it is clear now, that the external flux had to enter as a constant of integration, since it adds to the total flux through the inductance and therefore to the energy; keep in mind that generating the external flux through the loop consumed energy. The external flux will be important later, because it will enable us to manipulate certain properties of circuits from the outside.

To acquire the quantum mechanics of the LC circuit we transform from $\mathcal{L}_{\mathrm{LC}}$ to the Hamiltonian

$$H_{\mathrm{LC}}(p_\Phi, \Phi) = p_\Phi \dot{\Phi} - \mathcal{L}_{\mathrm{LC}} = \frac{1}{2C}p_\Phi^2 + \frac{1}{2L}(\Phi - \Phi_0)^2, \tag{2.3}$$

with the canonical momentum $p_\Phi = \frac{\partial \mathcal{L}_{\mathrm{LC}}}{\partial \dot{\Phi}}$. Treating Φ_0 as a constant that just shifts the potential and understanding Φ and p_Φ as operators with the canonical commutation relations $[\Phi, p_\Phi] = \mathrm{i}\hbar$, we of course know that this is a quantum harmonic oscillator with frequency $\omega = \frac{1}{\sqrt{LC}}$. This is no surprise as the LC circuit is already classically well known to be a harmonic oscillator. This scheme of starting with the classical Lagrangian, transforming to the Hamiltonian, and introducing quantum mechanics through canonical commutation relations has proven to consistently give correct results [8]. We start with the Lagrangian and not directly with a Hamiltonian because finding the correct canonical momentums and how they enter in the Hamiltonian is—as opposed to this example—often not obvious. We will observe this in later chapters (especially section 3.1.2).

One piece of equipment we still need is the Josephson junction. Here, for the voltage U across and the current I through the junction, the Josephson equations

$$U = \frac{\hbar}{2e}\dot{\phi}, \text{ and } I = I_{\mathrm{c}} \sin(\phi), \tag{2.4}$$

hold, where I_{c} is the critical current (a structural constant) of the junction, and ϕ is the phase difference of the superconducting wave functions on each side of the junction. With the integration of such junctions in a circuit it makes sense to switch our variables in the Lagrangian from flux Φ to phase ϕ by combining the identities for the voltage $\dot{\Phi} = U = \frac{\hbar}{2e}\dot{\phi}$, hence $\Phi = \frac{\hbar}{2e}\phi$. One can then check that a Josephson junction J will contribute a potential

$$V_J = \int U I \,\mathrm{d}t = \frac{\hbar}{2e} I_{\mathrm{c}} \int \sin(\phi)\dot{\phi}\,\mathrm{d}t = -\frac{\hbar}{2e} I_{\mathrm{c}} \cos(\phi) \tag{2.5}$$

to the Lagrangian. The phase is constant in every piece of wire in a circuit, due to long coherence lengths in superconductors, and elements in parallel will have the same phase

Contributions to the Lagrangian:

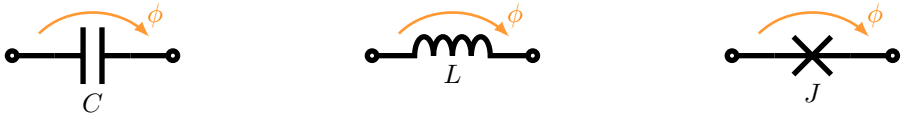

Kinetic energy:	Potential:	Potential:
$T_C = (\frac{\hbar}{2e})^2 \frac{1}{2} C\dot{\phi}^2$	$V_L = (\frac{\hbar}{2e})^2 \frac{1}{2L}(\phi - \phi_0)^2$	$V_J = -\frac{\hbar}{2e} I_\mathrm{c} \cos(\phi)$

Figure 2.2: Circuit diagrams of a capacitance C, an inductance L and a Josephson junction J (with critical current I_c) with a phase difference of ϕ occurring across each element. The elements then contribute a kinetic or potential term to the Lagrangian $\mathcal{L} = T - V$ as listed, where T is the sum of all kinetic energies, and V is the sum of all potentials.

difference across them; analogously to voltage in the classical treatment of electrical circuits.

Also note that if we introduce the phase in the Lagrangian of the LC circuit

$$\mathcal{L}_\mathrm{LC} = \left(\frac{\hbar}{2e}\right)^2 \frac{1}{2} C\dot{\phi}^2 - \left(\frac{\hbar}{2e}\right)^2 \frac{1}{2L}(\phi - \phi_0)^2, \tag{2.6}$$

when we transform again to the Hamiltonian, we get

$$H_\mathrm{LC} = \frac{(2e)^2}{2C} N^2 + \left(\frac{\hbar}{2e}\right)^2 \frac{1}{2L}\phi^2, \tag{2.7}$$

where we used $N = \frac{1}{\hbar}\frac{\partial \mathcal{L}}{\partial \dot{\phi}}$, so $[\phi, N] = \mathrm{i}$. In comparison with the energy $\frac{Q^2}{2C}$ of a capacitor, we find the physical meaning of the canonical momentum to the phase: the operator N counts the number of charges (in units of $2e$).

Summary of the Method

For a better overview, let us condense how we will handle the superconducting circuits in the following. Each isolated piece of wire will be given a distinct phase. A phase difference ϕ across a conductance C will lead to a kinetic term $T_C = (\frac{\hbar}{2e})^2 \frac{1}{2} C\dot{\phi}^2$, across an inductance L it will lead to a potential term $V_L = (\frac{\hbar}{2e})^2 \frac{1}{2L}(\phi - \phi_0)^2$ (with an external flux $\Phi_0 = \frac{\hbar}{2e}\phi_0$ present), and across a Josephson junction J it will give a potential $V_J = -\frac{\hbar}{2e} I_\mathrm{c} \cos(\phi)$; as taken together in figure 2.2. The terms of all elements in the circuit will then be summed up in the Lagrangian $\mathcal{L} = T - V$ depending on all the phases and their time derivatives, where of course T is the sum of all kinetic terms and V of all potential terms. The Lagrangian will then be transformed to a Hamiltonian, where the new canonical variables will be treated as operators with canonical commutation relations to study the quantum mechanics of the circuit.

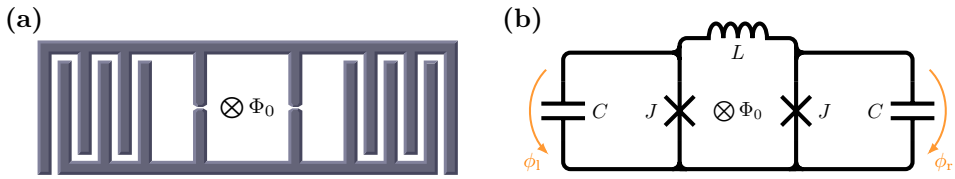

Figure 2.3: **(a)** Schematic of a tunable transmon qubit. The two Josephson junctions are sketched as small disruptions in the superconducting metal. They form a loop containing a magnetic flux Φ_0. The junctions are shunted by two large finger capacitors, which are interlacing structures of the superconductors with a relatively large capacitance due to the geometry. The size of the hole structure is about 100 µm. **(b)** The corresponding circuit diagram with the Josephson junctions J, the capacitances C in parallel, and the intrinsic inductance L of the loop. The phase differences across the junctions (and capacitances) are labeled ϕ_l and ϕ_r.

2.3 The Tunable Transmon Qubit

The fundamental structures of our quantum emulator are going to be superconducting qubits. The question was what type of qubits we would like to use, because there are many options for the implementation of a qubit in a superconducting circuit [10, 8]. The decision fell for the transmon, which was originally made popular by researchers in Yale [11]. It has great potential for a useful realization of the emulator in near future as the coherence times of modern transmon designs are already quite high [12, 13] and could therefore allow for a long calculation time of the emulator while still producing a trustworthy result. We also want to be able to access the transmons from the external, therefore we will be using tunable transmons.

The construction of a tunable transmon is shown in figure 2.3 (a): It consists of a superconducting loop containing two Josephson junctions, with two big finger capacitors as shunt capacitances in parallel. This is the main feature of the transmon, because these capacitances reduce the effects of noise on the charge operator, decreasing the fluctuations of the energy levels. A constant external magnetic flux Φ_0 is applied through the loop, which will be our tool for manipulation from the outside. The size of the structure is typically of the order of 100 µm. Figure 2.3 (b) then shows the circuit diagram of this structure with the two Josephson junctions J (with critical current I_c) forming a loop which has an inductance L, and the capacitances C in parallel, where the intrinsic geometric capacitances of the junctions have been absorbed into C. The phases across these two junctions (and their shunt capacitances) are denoted ϕ_l and ϕ_r, for the external flux we introduce $\phi_0 = \frac{2e}{\hbar}\Phi_0$. With the work of the previous section (see figure 2.2) we can write down the Lagrangian of the system to be

$$\mathcal{L}_\mathrm{T} = \left(\frac{\hbar}{2e}\right)^2 \frac{1}{2} C(\dot{\phi}_\mathrm{l}^2 + \dot{\phi}_\mathrm{r}^2)^2 + \frac{\hbar}{2e} I_\mathrm{c}(\cos(\phi_\mathrm{l}) + \cos(\phi_\mathrm{r}))^2 - \left(\frac{\hbar}{2e}\right)^2 \frac{1}{2L}(\phi_\mathrm{l} - \phi_\mathrm{r} - \phi_0)^2. \tag{2.8}$$

Using addition theorems for the cosine we get $\cos(\phi_\mathrm{l}) + \cos(\phi_\mathrm{r}) = 2\cos(\frac{\phi_\mathrm{l}+\phi_\mathrm{r}}{2})\cos(\frac{\phi_\mathrm{l}-\phi_\mathrm{r}}{2})$,

introducing new variables $\phi = \frac{1}{2}(\phi_\mathrm{l} + \phi_\mathrm{r})$ and $\phi_- = \frac{1}{2}(\phi_\mathrm{l} - \phi_\mathrm{r} - \phi_0)$, using $\dot{\phi}_0 = 0$ we get

$$\mathcal{L}_\mathrm{T} = \left(\frac{\hbar}{2e}\right)^2 C(\dot{\phi}^2 + \dot{\phi}_-^2) + \frac{\hbar}{e} I_\mathrm{c} \cos(\phi) \cos(\phi_- + \frac{\phi_0}{2}) - \left(\frac{\hbar}{2e}\right)^2 \frac{2}{L} \phi_-^2, \tag{2.9}$$

which transforms to the Hamiltonian

$$H_\mathrm{T} = E_C(N^2 + N_-^2) - E_J \cos(\phi) \cos(\phi_- + \frac{\phi_0}{2}) + \frac{E_L}{2} \phi_-^2, \tag{2.10}$$

with $N_{(-)} = \frac{1}{\hbar} \frac{\partial \mathcal{L}_\mathrm{T}}{\partial \dot{\phi}_{(-)}}$ as well as $E_C = \frac{e^2}{C}$, $E_J = \frac{\hbar}{e} I_\mathrm{c}$ and $E_L = (\frac{\hbar}{e})^2 \frac{1}{L}$.

The inductance of the loop is very small and therefore E_L is very large. Compared to E_J it is typically over three orders of magnitude larger. For the degree of freedom associated with ϕ_-, this means that the cosine potential term can be neglected for this coordinate and we find a harmonic oscillator

$$H_- = E_C N_-^2 + \frac{E_L}{2} \phi_-^2. \tag{2.11}$$

Again, since E_L is such a large energy scale, it leads to this oscillator not being excited by processes in the circuit or the environment. Therefore we can effectively set it to zero and end up with an effective Hamiltonian

$$H_\mathrm{T} = E_C N^2 - E_J \cos(\frac{\phi_0}{2}) \cos(\phi). \tag{2.12}$$

So the transformation of variables and fixing of the high-energy degree of freedom introduces the external phase ϕ_0 as a prefactor in the potential of the remaining degree of freedom. This is in the end our tool to manipulate our transmon qubit from the outside.

The remaining degree of freedom is an anharmonic oscillator (compare it with a pendulum), and for the application as a qubit, which means a quantum two level system, only the ground state and the first excitation are relevant. This means small displacement so we can expand the cosine term for small ϕ giving

$$H_\mathrm{T} \approx E_C N^2 + \frac{E_J}{2} \cos(\frac{\phi_0}{2}) \phi^2, \tag{2.13}$$

where we ignored constant contributions to the Hamiltonian. This is now indeed a harmonic oscillator

$$H_\mathrm{T} = \hbar\omega (a^\dagger a + \frac{1}{2}), \tag{2.14}$$

with $\hbar\omega = \sqrt{2E_C E_J \cos(\phi_0/2)}$, as well as the identities $\phi = \frac{1}{\sqrt{2}} (\frac{2E_C}{E_J \cos(\phi_0/2)})^{\frac{1}{4}} (a^\dagger + a)$ and $N = \mathrm{i} \frac{1}{\sqrt{2}} (\frac{E_J \cos(\phi_0/2)}{2E_C})^{\frac{1}{4}} (a^\dagger - a)$. We now bring this in the usual form for qubits by projecting these expressions onto the space with basis $\{|0\rangle, |1\rangle\}$ of the ground state $|0\rangle$ and the first excited state $|1\rangle$. With the well-known Pauli operators $\sigma^x = |1\rangle\langle 0| + |0\rangle\langle 1|$, $\sigma^y = \mathrm{i}(|1\rangle\langle 0| - |0\rangle\langle 1|)$, and $\sigma^z = |1\rangle\langle 1| - |0\rangle\langle 0|$ we find (up to constant) the qubit

Hamiltonian

$$H_{\mathrm{T}} = \frac{1}{2}\epsilon\sigma^z, \tag{2.15}$$

with the qubit energy

$$\epsilon(\phi_0) = \sqrt{2E_C E_J \cos(\frac{\phi_0}{2})}, \tag{2.16}$$

depending on the external flux, and the representations

$$\phi = \frac{1}{\sqrt{2}}\Big(\frac{2E_C}{E_J\cos(\frac{\phi_0}{2})}\Big)^{\frac{1}{4}}\sigma^x, \tag{2.17}$$

$$N = \frac{1}{\sqrt{2}}\Big(\frac{E_J\cos(\frac{\phi_0}{2})}{2E_C}\Big)^{\frac{1}{4}}\sigma^y, \tag{2.18}$$

which will be of use later. Also needed in a later section is the identity

$$\begin{aligned}\cos(\phi) \approx 1 - \frac{\phi^2}{2} &= 1 - \frac{1}{4}\sqrt{\frac{2E_C}{E_J\cos(\frac{\phi_0}{2})}}({a^\dagger}^2 + a^2 + 2a^\dagger a + 1)\\ &= -\frac{1}{4}\sqrt{\frac{2E_C}{E_J\cos(\frac{\phi_0}{2})}}\sigma^z + \left(1 - \frac{1}{2}\sqrt{\frac{2E_C}{E_J\cos(\frac{\phi_0}{2})}}\right)\mathbb{1}.\end{aligned} \tag{2.19}$$

To finish this section, we will investigate the important property of anharmonicity. For this we study the contribution to the eigenenergies of the harmonic oscillator using first order perturbation theory by expanding the cosine to fourth order, giving a perturbing potential

$$H_1 = -\frac{E_J\cos(\frac{\phi_0}{2})}{24}\phi^4 = -\frac{E_C}{24}(a^\dagger + a)^4. \tag{2.20}$$

The correction to the n^{th} eigenenergy in first order is then given by $-\frac{E_C}{24}\langle n|(a^\dagger + a)^4|n\rangle$, where the matrix element is calculated by taking the six terms of the expansion of $(a^\dagger + a)^4$ with $a^\dagger$ and a each contributing twice and applying $[a, a^\dagger] = 1$ multiple times to end up with $\langle n|(a^\dagger + a)^4|n\rangle = \langle n|\big(6(a^\dagger a)^2 + 6a^\dagger a + 3|n\rangle$. Hence, we find the corrections to the eigenenergies to be

$$\langle n|H_1|n\rangle = -\frac{E_C}{8}\big(n(n+1) + \frac{1}{2}\big). \tag{2.21}$$

Therefore, the transition energy from the ground state to the first excited state is larger than the transition energy from the first to the second excited state; the difference of these transition energies is $\frac{E_C}{4}$. This is very important for the transmon to function as a viable two level system: Typically qubits might also have a level structure of more than two levels, however with the levels above the first two being energetically much higher, excitations of these levels can be neglected. As we can see this is not the case for the

transmon. Here transitions between the first two levels are always caused by resonant effects. The anharmonicity is then important as it protects from unwanted transitions from the first to the second excited state due to these transitions not meeting the correct resonance condition.

Now that the theory of transmons is established, we can continue by explaining how they will help building an emulator for fermionic systems.

2.4 Mapping Fermions onto Transmon Qubits

The key idea of a mapping between fermions and transmons is that fermionic states can either be occupied or non-occupied. So naturally one is tempted to represent every fermionic state by one qubit as a two level system. This naive thought does however ignore one fundamental problem: As the previous section 2.3 shows, the excitations of a transmon are bosonic. This means they have different commutation relations than fermionic excitations and can therefore in general not directly represent them. While there are in principle different qubit designs whose excitations are intrinsically fermionic, for example electrons on quantum dots or atoms in cold gases in optical traps, these realizations of qubits have other drawbacks towards transmons. So henceforth, when qubit excitations are mentioned, bosonic ones are meant.

Now let us look at the problem in more detail. When we imagine a system of fermions with n different states, and look at the creation and annihilation operators $c_j^\dagger$ and c_j with $j \in \{1, \dots, n\}$ for these states, they obey the anticommuting relations $\{c_j, c_{j'}^\dagger\} = \delta_{jj'}$ and $\{c_j, c_{j'}\} = \{c_j^\dagger, c_{j'}^\dagger\} = 0$. If we take a set of n transmons, the corresponding operators would be the raising and lowering operators σ_j^+ and σ_j^-, which can be expressed by $\sigma_j^\pm = \frac{1}{2}(\sigma_j^x \pm \mathrm{i}\sigma_j^y)$ with the Pauli operators σ_j^x and σ_j^y of the j^{th} qubit. For an individual qubit we find $\{\sigma_j^-, \sigma_j^+\} = 1$ and $\{\sigma_j^-, \sigma_j^-\} = \{\sigma_j^+, \sigma_j^+\} = 0$, however for $j \neq j'$ we find $[\sigma_j^-, \sigma_{j'}^+] = [\sigma_j^-, \sigma_{j'}^-] = [\sigma_j^+, \sigma_{j'}^+] = 0$, which are not the desired anticommuting relations we would need to equivalently represent fermionic states. One possible solution to this problem will be presented in the following.

2.4.1 The Jordan-Wigner Transformation

Pascual Jordan and Eugene Wigner introduced a mapping between spin operators and fermions already in 1928 [15]. Start again with a set of raising and lowering operators σ_j^+ and σ_j^-, where $j \in \{1, \dots, n\}$. One can then formally define operators

$$c_j = \mathrm{e}^{\mathrm{i}\pi\lambda_j}\sigma_j^-, \; c_j^\dagger = \mathrm{e}^{-\mathrm{i}\pi\lambda_j}\sigma_j^+, \tag{2.22}$$

with $\lambda_j = \sum_{l=1}^{j-1} \sigma_l^+\sigma_l^-$. If one uses the representation

$$c_j = (-1)^{\lambda_j}\sigma_j^-, \; c_j^\dagger = (-1)^{-\lambda_j}\sigma_j^+ \tag{2.23}$$

one can see what this transformation essentially does: The qubits are given numbers, and λ_j counts, how many qubits in front of the j^{th} one are excited. The lowering and raising operators are then adjusted by a minus sign for every excited preceding qubit. Using $\{\sigma_j^-, \sigma_j^+\} = 1$ and $\{\sigma_j^-, \sigma_j^-\} = \{\sigma_j^+, \sigma_j^+\} = 0$ as well as $[\sigma_j^-, \sigma_{j'}^+] = [\sigma_j^-, \sigma_{j'}^-] = [\sigma_j^+, \sigma_{j'}^+] = 0$ for $j \neq j'$, one can then check, that it holds that

$$\{c_j, c_{j'}^\dagger\} = \delta_{jj'} \text{ and } \{c_j, c_{j'}\} = \{c_j^\dagger, c_{j'}^\dagger\} = 0, \tag{2.24}$$

so the resulting operators are fermionic creation and annihilation operators; using this transformation, one is able to represent a fermionic system by a qubit system.

There is however a drawback to this method. If we would look at interactions between the j^{th} and j'^{th} fermionic states with $j < j'$, the interaction terms would be of the form

$$c_j^\dagger c_{j'} = \sigma_j^+ (-1)^{\lambda_{j'} - \lambda_j} \sigma_{j'}^-. \tag{2.25}$$

This means that it depends on the term $\lambda_{j'} - \lambda_j = \sum_{l=j}^{j'-1} \sigma_l^+ \sigma_l^-$, which in turn means that it depends not just on the spin operators with number j and j', but also on all the spin operators with numbers between j and j'. Therefore arbitrary interactions between only two fermions end up to map on interactions between possibly a large number of qubits. With our quantum emulator in mind, this means complicated multi-qubit interactions, which are not desired. On the other hand we find

$$\begin{aligned} c_j^\dagger c_j = \sigma_j^+ \sigma_j^- = \frac{1}{2}(\sigma_j^z + 1), \\ c_j^\dagger c_{j+1} = \sigma_j^+ \sigma_{j+1}^-. \end{aligned} \tag{2.26}$$

If you look closely you will realize that these equations give you the tools to conveniently transform one-dimensional fermionic systems that only have nearest neighbor interactions between the fermions. Jordan and Wigner also used their transformation to study one-dimensional systems, e. g., they worked with the equivalence between the one-dimensional Heisenberg model, resp. the Heisenberg spin chain, and a chain of spinless fermions with only next neighbor interaction.

But again, arbitrary interactions are difficult to realize, which will especially be the case in dimensions greater than one. An interesting model, which can still be transformed without having to introduce multi-qubit interactions is the Fermi-Hubbard model in one dimension. This is the model which will be analyzed in this thesis.

2.4.2 Mapping of the Fermi-Hubbard Model in One Dimension

The Fermi-Hubbard model is of course a significant model in physics, especially condensed matter physics. As an extension to the tight-binding model, it serves as a simple description of systems of strongly correlated electrons in a narrow band structure. It has applications for example to describe transitions between a conducting and an isolating state of a system. Using mean field approximation, it can explain ferromag-

netism within the Stoner model. Recently it has also been considered as mechanism for high-temperature superconductivity. The one-dimensional version of the Fermi-Hubbard Hamiltonian could serve as a model for chains of atoms in cold gases, an approximation for the behavior of certain molecules, or as a description of systems on the nanoscale, which are effectively one-dimensional due to geometric confinements. One should mention at this point that there exists an analytic solution for the one (and infinite) dimensional case. The solution in one dimension was published by Lieb and Wu in 1968 [16] using a Bethe ansatz. While a number of properties could be extracted from this solution [17, 18], using constrains like half-filling or looking at thermodynamic limits, a general time evolution for example would still be impractical to extract from this solution, as the representation of the eigenstates of a system with n sites contains a sum over $(2n)!$ different terms. So an emulator of this model could still produce valuable results.

The Hamiltonian of the one-dimensional Fermi-Hubbard model with n sites, on-site energy U, transfer energy t, with interaction only between next neighbors and without spin-flip reads

$$H_{\mathrm{FH}} = U \sum_{j=1}^{n} c_{j,\uparrow}^{\dagger} c_{j,\uparrow} c_{j,\downarrow}^{\dagger} c_{j,\downarrow} - t \sum_{j=1}^{n-1} \sum_{s=\uparrow,\downarrow} (c_{j,s}^{\dagger} c_{j+1,s} + c_{j+1,s}^{\dagger} c_{j,s}), \tag{2.27}$$

where $c_{j,s}^{\dagger}$ and $c_{j,s}$ are fermionic creation and annihilation operators. We then introduce $2n$ qubits to represent these fermionic states, where we label their Pauli operators as well as their raising and lowering operators accordingly by $\sigma_{j,s}^{(\cdot)}$, where $j \in \{1, \ldots, n\}$ and $s \in \{\uparrow, \downarrow\}$.

We will now perform the Jordan-Wigner transformation on these spin operators. Formally, since one has to number all operators consecutively, imagine for the moment a numbering where we would change the indices with a mapping $(j, \uparrow) \mapsto j$ and $(j, \downarrow) \mapsto j + n$. Performing the Jordan-Wigner transformation using the identities (2.26) we find

$$\begin{aligned} H_{\mathrm{FH}} &= U \sum_{j=1}^{n} c_{j,\uparrow}^{\dagger} c_{j,\uparrow} c_{j,\downarrow}^{\dagger} c_{j,\downarrow} - t \sum_{j=1}^{n-1} \sum_{s=\uparrow,\downarrow} (c_{j,s}^{\dagger} c_{j+1,s} + c_{j+1,s}^{\dagger} c_{j,s}) \\ &= \frac{U}{4} \sum_{j=1}^{n} (\sigma_{j,\uparrow}^{z} + 1)(\sigma_{j,\downarrow}^{z} + 1) - t \sum_{j=1}^{N-1} \sum_{s=\uparrow,\downarrow} (\sigma_{j,s}^{+} \sigma_{j+1,s}^{-} + \sigma_{j+1,s}^{+} \sigma_{j,s}^{-}), \end{aligned} \tag{2.28}$$

so we now have a qubit system, which resembles the Fermi-Hubbard model in one dimension.

Let us further analyze this system. We will start with the first sum

$$\frac{U}{4} \sum_{j=1}^{n} (\sigma_{j,\uparrow}^{z} + 1)(\sigma_{j,\downarrow}^{z} + 1) = \frac{U}{4} \sum_{j=1}^{n} \sigma_{j,\uparrow}^{z} \sigma_{j,\downarrow}^{z} + \frac{U}{4} \sum_{j=1}^{n} (\sigma_{j,\uparrow}^{z} + \sigma_{j,\downarrow}^{z}) + n \frac{U}{4}. \tag{2.29}$$

If we would like to have particle conservation in the fermionic system, this would result in the second sum of the right hand side to be constant, as it is a measure of the overall

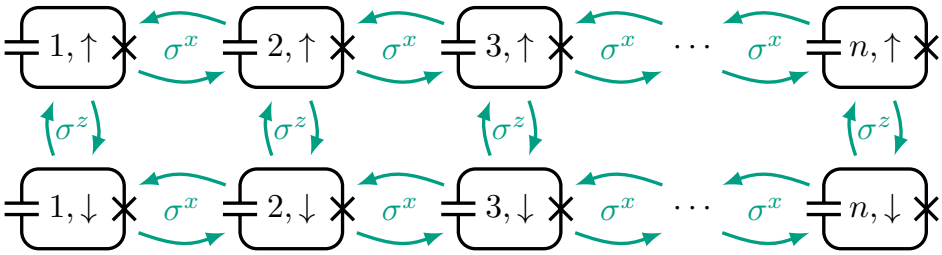

Figure 2.4: A sketch of a system of transmons that provide a Hamiltonian, that is equivalent to the Fermi-Hubbard model in one dimension. It consists of two chains of n qubits, which represent the spin-up and spin-down states of the Fermi-Hubbard model. Neighboring qubits in each chain are coupled via their σ^x operators to accomplish the transfer integral terms of the Fermi-Hubbard model with nearest neighbor interaction. Laying out the two chains next to each other with opposing transmons being coupled via σ^z gives the on-site energy terms.

qubit excitations. Since $n\frac{U}{4}$ is trivially constant as well, we end up with the equivalence

$$\frac{U}{4}\sum_{j=1}^{n}(\sigma_{j,\uparrow}^{z}+1)(\sigma_{j,\downarrow}^{z}+1) \sim \frac{U}{4}\sum_{j=1}^{n}\sigma_{j,\uparrow}^{z}\sigma_{j,\downarrow}^{z}. \tag{2.30}$$

To tackle the remaining sum of the qubit system, consider all qubits to have the same energy splitting ϵ between their two levels and the parameter t to be small compared to ϵ. As a result, terms of the form $t\sigma_{j,s}^{+}\sigma_{j+1,s}^{+}$ and $t\sigma_{j,s}^{-}\sigma_{j+1,s}^{-}$ will effectively vanish since the transitions between states caused by such terms violate energy conservation. This means that in this limit the second sum of our transmon system has the similarity

$$\begin{aligned} t\sum_{j=1}^{n-1}\sum_{s=\uparrow,\downarrow}(\sigma_{j,s}^{+}\sigma_{j+1,s}^{-}+\sigma_{j+1,s}^{+}\sigma_{j,s}^{-}) &\sim t\sum_{j=1}^{n-1}\sum_{s=\uparrow,\downarrow}(\sigma_{j,s}^{+}+\sigma_{j,s}^{-})(\sigma_{j+1,s}^{+}+\sigma_{j+1,s}^{-}) \\ &= t\sum_{j=1}^{n-1}\sum_{s=\uparrow,\downarrow}\sigma_{j,s}^{x}\sigma_{j+1,s}^{x}. \end{aligned} \tag{2.31}$$

With this result, we are at the point where we know how to build our quantum emulator in principle, as illustrated in figure 2.4: We take two chains of n transmon qubits, with neighboring transmons in each chain being coupled by a σ^x-type interaction. This represents the nearest neighbor interaction in each spin chain in the Fermi-Hubbard Hamiltonian. The two chains are placed next to each other and opposing transmons need to be coupled by their σ^z operators. If we consider equal transmons with energy splitting ϵ, and equal coupling energies g^x of the σ^x-type coupling and g^z for the coupling via σ^z respectively, the Hamiltonian H_{E} of such an emulator would read

$$H_{\mathrm{E}} = \sum_{j=1}^{n}\sum_{s=\uparrow,\downarrow}\frac{1}{2}\epsilon\sigma_{j,s}^{z} + g^{z}\sum_{j=1}^{n}\sigma_{j,\uparrow}^{z}\sigma_{j,\downarrow}^{z} + g^{x}\sum_{j=1}^{n-1}\sum_{s=\uparrow,\downarrow}\sigma_{j,s}^{x}\sigma_{j+1,s}^{x}, \tag{2.32}$$

where $\uparrow$ and $\downarrow$ of course denote the two mentioned chains. Finally in the also mentioned

limiting constrains of conservation of qubit excitations—hence particle conservation in the fermionic system—and $\frac{g^x}{\epsilon} \ll 1$, the above shows that this Hamiltonian is equivalent to the one-dimensional Fermi-Hubbard model, i. e. $H_{\mathrm{E}} \sim H_{\mathrm{FH}}$ with the identities

$$U = 4g^z \text{ and } t = -g^x. \tag{2.33}$$

Bear in mind at this point, that the constraint $\frac{g^x}{\epsilon} \ll 1$ is—in an otherwise ideal system—only technical and does not affect the range of the parameters U and t which can be emulated, since only the relation of U and t relative to each other is important for the properties of the Fermi-Hubbard model, which means that g^z just has to be adjusted in the correct fashion to resemble the desired set of parameters.

Lastly, having achieved to find an equivalent Hamiltonian, the subsequent task is clear: Methods of implementing the interactions via σ^x and σ^z between transmons need to be found. Also, the circuit designs of these implementations should be as simple as possible; this allows for an approach of building such an emulator in near future and is undoubtedly something to wish for. The next chapter will address these challenges and will also provide very satisfying options to meet them.

Chapter 3

Construction of the Emulator

Chapter 2 made the assignment for the construction of an emulator for the one-dimensional Fermi-Hubbard model based on transmons clear. Figure 2.4 shows how the qubits have to be coupled by their σ^z and σ^x operators.

This chapter provides circuit diagrams to realize these couplings, starting with the the σ^x-type interaction, followed by the more subtle mechanism to couple two transmons via σ^z. We will also give analytic expressions for the coupling energies depending on the quantities in the circuit.

We will conclude by briefly discussing the possibility of the experimental realization of the found circuit diagrams to convince ourselves, that the discussed mechanisms are in fact manufacturable.

3.1 Coupling of Tunable Transmons via σ^x

The first type of transmon coupling we address is the coupling via their σ^x operators. It is quite clear that using inductances or capacitances to connect individual qubits, we will obtain linear coupling terms between their phase or charge operators, which can be seen from the terms they contribute in the Lagrangian summarized in figure 2.2 and the fact that the charge operator is related to the time derivative of the phase. Looking at the equations (2.17) and (2.18), we then see how this will give linear coupling via σ^x or σ^y; note that in the limit of small coupling these interactions are effectively equivalent, which will be explained in more detail in the following section 3.1.2.

This is also not a new insight, such coupling has already been established in experiment, especially since—as section 4.1.3 will explain—this type of coupling is also used to flip qubits from the ground into the excited state for initialization [11].

We will now proceed to carry out the calculations for the two coupling methods in detail in order to understand the mechanisms properly. We will then also be able to give formulas to calculate the coupling energies depending on the values of the circuit elements. As a last step we will compare the two methods of coupling to see why the capacitative coupling is the better choice for an experimental realization.

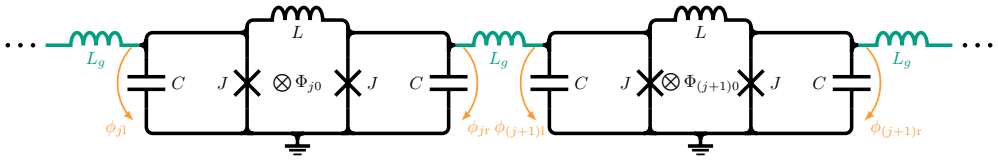

Figure 3.1: The circuit diagram of a chain of coupled identical transmons. They are each made out of a loop containing two Josephson junctions J (with critical current I_c) and intrinsic inductance L. The junctions are shunted by the capacitances C. Each of the n transmons can be tuned by an individual external flux $\Phi_{j0} = \frac{\hbar}{2e}\phi_{j0}$. The phases across the junctions of the j^{th} qubit are denoted $\phi_{j\mathrm{l}}$ and $\phi_{j\mathrm{r}}$. The bottom parts of the transmons are connected to ground and the upper parts are connected through coupling inductances L_g between neighboring qubits. For large values of L_g, this setup gives a small σ^x coupling between the qubits.

3.1.1 Coupling through Inductances

The first option of linear coupling between transmons we investigate is the coupling by additional inductances. For this, consider a chain of n identical tunable transmons which are then coupled by inductances, which is shown in figure 3.1. Each transmon consists of two Josephson junctions J (with critical current I_c) and shunt capacities C, the inductance of the loop is labeled L. Each transmon can be tuned individually with external magnetic flux $\Phi_{j0} = \frac{\hbar}{2e}\phi_{j0}$ at the j^{th} qubit. The coupling is done via inductances L_g. The phase differences across the junctions of the j^{th} transmon are denoted $\phi_{j\mathrm{l}}$ and $\phi_{j\mathrm{r}}$.

Before we continue deriving the Lagrangian, note that we set the lower parts of all transmons to ground. For a start, one could simply connect this part to ground in an experiment, or one could wire the lower parts together which is equivalent in this case. If one does not do that, one has to account for the phase differences between these parts of the circuit as they will enter in the potential energies of the coupling inductances. One can for example introduce ground as reference and connect the qubits to ground through a capacitance; this would always be the case in a real experiment if the qubits on the chip would not be wired to ground directly anyhow. These extra phases in the Lagrangian would either not have an own dynamic at all, or the dynamic can be decoupled from the system in a way. In the end, such setups would just lead to the same circuit as in figure 3.1, with redefined quantities. Therefore, we can stick with this circuit diagram without making any qualitative mistake. In a more precise calculation for an experiment one would have to adjust to the detailed experimental realization; but again, to see how the coupling works in general, this circuit covers all that is needed.

Let us derive the Lagrangian now. For this, we use our findings in figure 2.2 of section 2.2.1, so that, with the help of the circuit diagram in figure 3.1, we can immediately

write down the Lagrangian

$$\mathcal{L}_L^x = \sum_{j=1}^{n} \left(\left(\frac{\hbar}{2e}\right)^2 \frac{1}{2} C(\dot{\phi}_{j\mathrm{l}}^2 + \dot{\phi}_{j\mathrm{r}}^2) + \frac{\hbar}{2e} I_\mathrm{c}(\cos(\phi_{j\mathrm{l}}) + \cos(\phi_{j\mathrm{r}})) \right.$$
$$\left. - \left(\frac{\hbar}{2e}\right)^2 \frac{1}{2L} (\phi_{j\mathrm{l}} - \phi_{j\mathrm{r}} - \phi_{j0})^2 \right) - \sum_{j=1}^{n-1} \left(\frac{\hbar}{2e}\right)^2 \frac{1}{2L_g} (\phi_{j\mathrm{r}} - \phi_{(j+1)\mathrm{l}})^2, \quad (3.1)$$

where the first sum consists of the usual qubit terms and the second sum accounts for the coupling. We continue analogously to section 2.3 and introduce the phases $\phi_j = \frac{1}{2}(\phi_{j\mathrm{l}} + \phi_{j\mathrm{r}})$ as well as $\phi_{j-} = \frac{1}{2}(\phi_{j\mathrm{l}} - \phi_{j\mathrm{r}} - \phi_{j0})$, and also use the addition theorems for the cosine and arrive at

$$\mathcal{L}_L^x = \sum_{j=1}^{n} \left(\left(\frac{\hbar}{2e}\right)^2 C(\dot{\phi}_j^2 + \dot{\phi}_{j-}^2) + \frac{\hbar}{e} I_\mathrm{c} \cos(\phi_{j-} + \frac{\phi_{j0}}{2}) \cos(\phi_j) - \left(\frac{\hbar}{2e}\right)^2 \frac{2}{L} \phi_{j-}^2 \right)$$
$$- \sum_{j=1}^{n-1} \left(\frac{\hbar}{2e}\right)^2 \frac{1}{2L_g} \left(\left(\phi_j - \phi_{j-} - \frac{\phi_{j0}}{2}\right) - \left(\phi_{j+1} + \phi_{(j+1)-} + \frac{\phi_{(j+1)0}}{2}\right) \right)^2, \quad (3.2)$$

which, with $N_j = \frac{1}{\hbar} \frac{\partial \mathcal{L}_L^x}{\partial \dot{\phi}_j}$ and $N_{j-} = \frac{1}{\hbar} \frac{\partial \mathcal{L}_L^x}{\partial \dot{\phi}_{j-}}$, easily transforms to the Hamiltonian

$$H_L^x = \sum_{j=1}^{n} \left(E_C(N_j^2 + N_{j-}^2) - E_J \cos(\phi_{j-} + \frac{\phi_{j0}}{2}) \cos(\phi_j) + \frac{1}{2} E_L \phi_{j-}^2 \right)$$
$$+ \sum_{j=1}^{n-1} \frac{1}{8} E_{L_g} \left(\left(\phi_j - \phi_{j-} - \frac{\phi_{j0}}{2}\right) - \left(\phi_{j+1} + \phi_{(j+1)-} + \frac{\phi_{(j+1)0}}{2}\right) \right)^2, \quad (3.3)$$

with $E_C = \frac{e^2}{C}$, $E_J = \frac{\hbar}{e} I_\mathrm{c}$ and $E_{L_{(g)}} = (\frac{\hbar}{e})^2 \frac{1}{L_{(g)}}$.

In section 2.4.2 we established that we need to operate in the limit of small coupling for the σ^x-type coupling, hence we need to have $E_{L_g} \ll E_J$, which means the coupling inductances need to be very large. Section 2.3 established that due to the small intrinsic inductance in the loop of the transmon, E_L is a dominant energy scale towards the qubit excitation energy. Combining this, we find that E_L stays dominant in this system of coupled transmons, so we can proceed as in section 2.3 and fix the degrees of freedom associated with this high energy to zero, hence $\phi_{j-}, N_{j-} \approx 0$, as excitations of these degrees of freedom are unlikely. This gives

$$H_L^x = \sum_{j=1}^{n} \left(E_C N_j^2 - E_J \cos(\frac{\phi_{j0}}{2}) \cos(\phi_j) \right)$$
$$+ \sum_{j=1}^{n-1} \frac{1}{8} E_{L_g} \left(\left(\phi_j - \frac{\phi_{j0}}{2}\right) - \left(\phi_{j+1} + \frac{\phi_{(j+1)0}}{2}\right) \right)^2$$
$$= \sum_{j=1}^{n} \frac{1}{2} \epsilon_j \sigma_j^z + \sum_{j=1}^{n-1} \frac{1}{8} E_{L_g} \left(\left(\alpha_j^x \sigma_j^x - \frac{\phi_{j0}}{2}\right) - \left(\alpha_{j+1}^x \sigma_{j+1}^x + \frac{\phi_{(j+1)0}}{2}\right) \right)^2, \quad (3.4)$$

where we used the equations (2.15) and (2.17) to transform into the qubit eigenbasis with $\epsilon_j = \sqrt{2E_C E_J \cos(\phi_{j0}/2)}$ and $\alpha_j^x = \frac{1}{\sqrt{2}}(\frac{2E_C}{E_J \cos(\phi_{j0}/2)})^{\frac{1}{4}}$.

Let us study the coupling term

$$H_1^x = \sum_{j=1}^{n-1} \frac{1}{8} E_{L_g} \left(\left(\alpha_j^x \sigma_j^x - \frac{\phi_{j0}}{2} \right) - \left(\alpha_{j+1}^x \sigma_{j+1}^x + \frac{\phi_{(j+1)0}}{2} \right) \right)^2 \tag{3.5}$$

in more detail. Remember that, once they are set, the external phases are constant, and also that $(\sigma^x)^2 = \mathbb{1}$, so if we expand this expression and neglect constant contributions we find

$$H_1^x = \sum_{j=1}^{n-1} \frac{1}{4} E_{L_g} \big(- \alpha_j^x (\phi_{j0} + \phi_{(j+1)0}) \sigma_j^x + \alpha_{j+1}^x (\phi_{j0} + \phi_{(j+1)0}) \sigma_{j+1}^x - \alpha_j^x \alpha_{j+1}^x \sigma_j^x \sigma_{j+1}^x \big). \tag{3.6}$$

The last term yields our desired σ^x-type coupling between the transmons. To address the other two terms, keep in mind that our transmons are considered equal and that they need to be tuned to all have the same energy splitting for the emulation of the Fermi-Hubbard model. This is because the energy of the sum of all qubit excitations has to be constant, as mentioned in section 2.4.2. This means that our external phases ϕ_{j0} as well as the coefficients α_j^x should pairwise be approximately equal for every $j \in \{1, \ldots, n\}$. This in turn means that, if you look closely, you can see how the first two terms yield a telescoping sum

$$\sum_{j=1}^{n-1} \frac{1}{4} E_{L_g} \big(- \alpha_j^x (\phi_{j0} + \phi_{(j+1)0}) \sigma_j^x + \alpha_{j+1}^x (\phi_{j0} + \phi_{(j+1)0}) \sigma_{j+1}^x \big) \approx 0, \tag{3.7}$$

which vanishes under these conditions, when we also neglect the boundary terms (they would also cancel if one decides to use continuous boundary conditions). Note that even if some terms do not completely cancel out to zero, in any case it holds that $\frac{E_{L_g}}{\epsilon_j} \ll 1$, hence the off-diagonal terms that add up to the individual qubit terms would only cause tiny rotations of the eigenstates of each qubit out of the z-axis. Therefore the approximation in equation (3.7) is valid and we end up with the effective Hamiltonian

$$H_L^x = \sum_{j=1}^{n} \frac{1}{2} \epsilon_j \sigma_j^z + \sum_{j=1}^{n-1} g_j \sigma_j^x \sigma_{j+1}^x, \tag{3.8}$$

with $g_j = -\frac{1}{4} E_{L_g} \alpha_j^x \alpha_{j+1}^x = -\frac{1}{8} E_{L_g} \sqrt{\frac{2E_C}{E_J}} (\frac{1}{\cos(\phi_{j0}/2) \cos(\phi_{(j+1)0}/2)})^{\frac{1}{4}}$. So if we, for all $j \in \{1, \ldots, n\}$, write $\phi_{j0} = \phi_0$ resulting in $\epsilon_j = \epsilon = \sqrt{2E_C E_J \cos(\phi_0/2)}$, since our external fields are ideally equal, we get

$$H_L^x = \sum_{j=1}^{n} \frac{1}{2} \epsilon \sigma_j^z + g_L^x \sum_{j=1}^{n-1} \sigma_j^x \sigma_{j+1}^x, \tag{3.9}$$

with the coupling strength

$$g_L^x = -\frac{1}{8} E_{L_g} \sqrt{\frac{2E_C}{E_J \cos(\frac{\phi_0}{2})}} = -\frac{1}{8} \frac{\epsilon}{E_J \cos(\frac{\phi_0}{2})} E_{L_g}, \tag{3.10}$$

which is precisely the form desired from equation (2.32) to emulate the hopping terms in the Fermi-Hubbard model with transfer energy $t = -g_L^x$.

This shows how the coupling through an inductance—one of the linear elements of superconducting circuits—leads to an interaction via σ^x, like predicted. We will now proceed by checking how coupling through capacitances will work, to be able to compare the different results.

3.1.2 Coupling through Capacitances

A Mathematical Excursus

Before we begin to study the circuit of tunable transmons coupled via capacitances, we will briefly face a mathematical problem that will reappear in the later calculation. For this, we define the $n \times n$ matrices Q_q and A_q for $q \in (-\frac{1}{2}, \frac{1}{2})$ by

$$Q_q = \begin{pmatrix} 0 & q & 0 & 0 & \cdots \\ q & 0 & q & 0 & \cdots \\ 0 & q & 0 & q & \cdots \\ 0 & 0 & q & 0 & \cdots \\ \vdots & \vdots & \vdots & \vdots & \ddots \end{pmatrix}, \text{ and } A_q = \begin{pmatrix} 1 & -q & 0 & 0 & \cdots \\ -q & 1 & -q & 0 & \cdots \\ 0 & -q & 1 & -q & \cdots \\ 0 & 0 & -q & 1 & \cdots \\ \vdots & \vdots & \vdots & \vdots & \ddots \end{pmatrix}, \tag{3.11}$$

so Q_q is a matrix with value q on the first off-diagonals and is zero for every other matrix element, and $A_q = \mathbb{1} - Q_q$ is a tridiagonal matrix where the diagonal elements are ones and the elements of the first off-diagonal have the value $-q$; the rest being zero. In analogy to the geometric series $\frac{1}{1-q} = \sum_{m=0}^{\infty} q^m$ for $q \in (-1, 1)$, for values of $q \in (-\frac{1}{2}, \frac{1}{2})$ one can show that the series $\sum_{m=0}^{\infty} Q_q^m$ converges as well. Since

$$(\mathbb{1} + Q_q + Q_q^2 + \cdots + Q_q^m)(\mathbb{1} - Q_q) = \mathbb{1} - Q_q^{m+1} = \mathbb{1} + \mathcal{O}(q^{m+1}), \tag{3.12}$$

where we made use of the obvious fact that the matrix elements of Q_q^m are either zero or proportional to q^m for all natural m, we can see that the geometric series in Q_q gives the inverse matrix to $\mathbb{1} - Q_q$, hence

$$A_q^{-1} = \sum_{m=0}^{\infty} Q_q^m. \tag{3.13}$$

To check in more detail how the inverse of A_q looks like, one can write the matrix

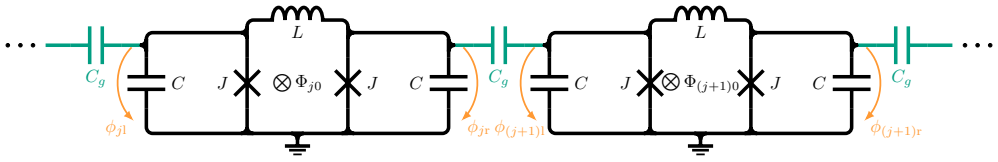

Figure 3.2: Again a circuit diagram of a chain of coupled identical transmons, with Josephson junctions J (with critical current I_c), shunt capacitances C and loop inductance L. They are again individually tunable though external fluxes $\Phi_{j0} = \frac{\hbar}{2e}\phi_{j0}$, and the phase differences across the junctions of the j^{th} qubit are denoted $\phi_{j\mathrm{l}}$ and $\phi_{j\mathrm{r}}$. The bottom parts of the transmons are grounded, but this time the top parts of the transmons are coupled by capacitances C_g between neighboring transmons. For small values of C_g, this leads to a σ^x-type interaction between the transmons, with a coupling strength proportional to the fraction $\frac{C_g}{C}$.

elements of Q_q as $(Q_q)_{ij} = q(\delta_{i,j-1} + \delta_{i,j+1})$ and therefore

$$(Q_q^2)_{ij} = \sum_{l=1}^{n} q^2(\delta_{i,k-1} + \delta_{i,k+1})(\delta_{k,j-1} + \delta_{k,j+1}) = q^2(\delta_{i,j-2} + 2\delta_{i,j} + \delta_{i,j+2}). \quad (3.14)$$

Inductively it is easy to see that the leading order of q on the m^{th} off-diagonal of A_q^{-1} will be q^m and the coefficient in front will be one. One can also check that the next nonvanishing order will be q^{m+2}. This gives the following expression for the matrix elements of A_q^{-1}:

$$(A_q^{-1})_{ij} = q^{|i-j|} + \mathcal{O}(q^{|i-j|+2}). \quad (3.15)$$

However, the result which we will utilize in particular in the upcoming calculation is the first order in q, as q will play the role of a small parameter. This can be denoted by the formula

$$A_q^{-1} = A_{-q} + \mathcal{O}(q^2). \quad (3.16)$$

The Circuit Calculation

We will now derive the quantum mechanics of a circuit analogous to the previous section 3.1.1, but replace the coupling inductances by capacitances. The circuit diagram is given in figure 3.2: Again we have a chain of n identical tunable transmons with Josephson junctions J (with critical current I_c) and shunt capacities C as well as the loop inductance L. The phase differences across the junctions of the j^{th} qubit are again denoted $\phi_{j\mathrm{l}}$ and $\phi_{j\mathrm{r}}$, and the external flux through the qubits are given by $\Phi_{j0} = \frac{\hbar}{2e}\phi_{j0}$. This time the qubits are however coupled by capacitances C_g. Again the bottom parts of the transmons are grounded, the reason why this is a valid treatment was already given in the previous section 3.1.1.

Applying our method to approach quantum circuits summarized in figure 2.2 on the

circuit diagram in figure 3.2, we obtain the Lagrangian

$$\mathcal{L}_C^x = \sum_{j=1}^{n} \left(\left(\frac{\hbar}{2e}\right)^2 \frac{1}{2} C(\dot{\phi}_{j\mathrm{l}}^2 + \dot{\phi}_{j\mathrm{r}}^2) + \frac{\hbar}{2e} I_c(\cos(\phi_{j\mathrm{l}}) + \cos(\phi_{j\mathrm{r}})) \right.$$
$$\left. - \left(\frac{\hbar}{2e}\right)^2 \frac{1}{2L} (\phi_{j\mathrm{l}} - \phi_{j\mathrm{r}} - \phi_{j0})^2 \right) + \sum_{j=1}^{n-1} \left(\frac{\hbar}{2e}\right)^2 \frac{1}{2} C_g (\dot{\phi}_{j\mathrm{r}} - \dot{\phi}_{(j+1)\mathrm{l}})^2. \quad (3.17)$$

Following the same strategy as in section 2.3 and 3.1.1, we introduce $\phi_j = \frac{1}{2}(\phi_{j\mathrm{l}} + \phi_{j\mathrm{r}})$ as well as $\phi_{j-} = \frac{1}{2}(\phi_{j\mathrm{l}} - \phi_{j\mathrm{r}} - \phi_{j0})$, use the addition theorems for the cosine and get

$$\mathcal{L}_C^x = \sum_{j=1}^{n} \left(\left(\frac{\hbar}{2e}\right)^2 C(\dot{\phi}_j^2 + \dot{\phi}_{j-}^2) + \frac{\hbar}{e} I_c \cos(\phi_{j-} + \frac{\phi_{j0}}{2}) \cos(\phi_j) - \left(\frac{\hbar}{2e}\right)^2 \frac{2}{L} \phi_{j-}^2 \right)$$
$$+ \sum_{j=1}^{n-1} \left(\frac{\hbar}{2e}\right)^2 \frac{1}{2} C_g \big((\dot{\phi}_j - \dot{\phi}_{j-}) - (\dot{\phi}_{j+1} + \dot{\phi}_{(j+1)-}) \big)^2, \quad (3.18)$$

where we made use of the fact that the external phases are constant, hence $\dot{\phi}_{j0} = 0$.

Just as in the previous section 3.1.1 it will turn out that the degrees of freedom associated with ϕ_{j-} can effectively be set to zero due to the steep potential resulting from the small inductance L; we will at this point already do this by fixing $\phi_{j-}, \dot{\phi}_{j-} \approx 0$. This way we have less terms in the Lagrangian to worry about for the transformation to the Hamiltonian. The Lagrangian now reads

$$\mathcal{L}_C^x = \sum_{j=1}^{n} \left(\left(\frac{\hbar}{2e}\right)^2 (C + C_g) \dot{\phi}_j^2 + \frac{\hbar}{e} I_c \cos(\frac{\phi_{j0}}{2}) \cos(\phi_j) \right) - \sum_{j=1}^{n-1} \left(\frac{\hbar}{2e}\right)^2 C_g \dot{\phi}_j \dot{\phi}_{j+1}$$
$$- \left(\frac{\hbar}{2e}\right)^2 \frac{1}{2} C_g (\dot{\phi}_1^2 + \dot{\phi}_n^2) \quad (3.19)$$

Remember that the coupling strength between the qubits must be small compared to the qubit energy as stated in section 2.4.2. We will see in the end that this will be achieved, if the coupling capacitances are small or to be more precise, if $\frac{C_g}{C} \ll 1$. If we operate in this regime, we can neglect the boundary terms $\frac{1}{2} C_g (\dot{\phi}_1^2 + \dot{\phi}_n^2)$, because $C + \frac{1}{2} C_g \approx C + C_g$ and it does only affect the boundary qubits anyhow. We also introduce the vector $\boldsymbol{\phi} = (\phi_1, \ldots, \phi_n)$ and the parameter $\lambda = \frac{1}{2} \frac{C_g}{C + C_g} \in (0, \frac{1}{2})$. One can then check that with the matrix A_λ, with the definition of the matrix given in equation (3.11) of the preliminary mathematical excursus, we can express the Lagrangian using matrix multiplication as

$$\mathcal{L}_C^x = \left(\frac{\hbar}{2e}\right)^2 (C + C_g) \dot{\boldsymbol{\phi}}^{\mathrm{T}} A_\lambda \dot{\boldsymbol{\phi}} + \sum_{j=1}^{n} \frac{\hbar}{e} I_c \cos(\frac{\phi_{j0}}{2}) \cos(\phi_j). \quad (3.20)$$

Since we want λ to be small, with the findings of equation (3.16), by neglecting terms of order $\mathcal{O}(\lambda^2)$, we can express the inverse of A_λ simply by $A_{-\lambda}$. With $\boldsymbol{N} = \frac{1}{\hbar} \frac{\partial \mathcal{L}_C^x}{\partial \dot{\boldsymbol{\phi}}}$ we

can now easily transform our Lagrangian to the Hamiltonian

$$\begin{aligned} H_C^x &= E_{\tilde{C}} \boldsymbol{N}^{\mathrm{T}} A_{-\lambda} \boldsymbol{N} - \sum_{j=1}^{n} E_J \cos(\frac{\phi_{j0}}{2}) \cos(\phi_j) \\ &= \sum_{j=1}^{n} \left(E_{\tilde{C}} N_j^2 - E_J \cos(\frac{\phi_{j0}}{2}) \cos(\phi_j) \right) + \sum_{j=1}^{n-1} 2E_{\tilde{C}} \lambda N_j N_{j+1}, \end{aligned} \tag{3.21}$$

with $\tilde{C} = C + C_g$, $E_{\tilde{C}} = \frac{e^2}{\tilde{C}}$ and $E_J = \frac{\hbar}{e} I_c$.

We resort to section 2.3 and equations (2.15) and (2.18) to see that the first sum will give us the qubit energy terms with qubit energies $\tilde{\epsilon}_j = \sqrt{2E_{\tilde{C}} E_J \cos(\phi_{j0}/2)}$ and we can use $N_j = \alpha_j^y \sigma_j^y$ with $\alpha_j^y = \frac{1}{\sqrt{2}} (\frac{E_J \cos(\phi_{j0}/2)}{2E_{\tilde{C}}})^{\frac{1}{4}}$. Now our Hamiltonian reads

$$H_C^x = \sum_{j=1}^{n} \frac{1}{2} \tilde{\epsilon}_j \sigma_j^z + \sum_{j=1}^{n} 2E_{\tilde{C}} \lambda \alpha_j^y \alpha_{j+1}^y \sigma_j^y \sigma_{j+1}^y. \tag{3.22}$$

As final step we address the fact that we now have σ^y operators in the coupling term instead of σ^x. This is however equivalent, one could just redefine the axes by a rotation. If we would like to be a bit more detailed about this issue, one can follow the same argument as in section 2.4.2: Because of the small prefactor $\lambda \ll 1$ in front of the coupling, the coupling energy is small compared to the qubit energy. As a remark, for a transmon we would already have $\frac{E_{\tilde{C}}}{\tilde{\epsilon}_j} \ll 1$ due to the big shunt capacitances. This means that terms $\lambda \sigma_j^+ \sigma_{j+1}^+$ and $\lambda \sigma_j^- \sigma_{j+1}^-$ can be neglected since they are not energy conserving, which means $\lambda \sigma_j^y \sigma_{j+1}^y = \lambda(\sigma_j^+ \sigma_{j+1}^- + \sigma_j^- \sigma_{j+1}^+ - \sigma_j^+ \sigma_{j+1}^+ - \lambda \sigma_j^- \sigma_{j+1}^-)$ is equivalent to $\lambda(\sigma_j^+ \sigma_{j+1}^- + \sigma_j^- \sigma_{j+1}^+ + \sigma_j^+ \sigma_{j+1}^+ + \lambda \sigma_j^- \sigma_{j+1}^-) = \lambda \sigma_j^x \sigma_{j+1}^x$. We can therefore write

$$H_C^x = \sum_{j=1}^{n} \frac{1}{2} \tilde{\epsilon}_j \sigma_j^z + \sum_{j=1}^{n-1} \tilde{g}_j \sigma_j^x \sigma_{j+1}^x, \tag{3.23}$$

with the coupling energy $\tilde{g}_j = 2E_{\tilde{C}} \lambda \alpha_j^y \alpha_{j+1}^y = \frac{1}{2} \lambda \sqrt{\tilde{\epsilon}_j \tilde{\epsilon}_{j+1}}$.

As a last step, we account for the fact that in the emulator all transmons will be tuned to have the same energy, therefore we set all external phases equal via $\phi_{j0} = \phi_0$ for all $j \in \{1, \ldots, n\}$, which leads to $\tilde{\epsilon}_j = \tilde{\epsilon} = \sqrt{2E_{\tilde{C}} E_J \cos(\phi_0/2)}$. We will also regard that in the regime of small coupling, hence $\frac{C_g}{C} \ll 1$, we find $\tilde{C} = C + C_g \approx C$; as a consequence we ignore the small shift of the energies and just drop the tilde in our terms, using the usual $\epsilon = \sqrt{2E_C E_J \cos(\phi_0/2)}$ with $E_C = \frac{e^2}{C}$ and $\lambda = \frac{1}{2} \frac{C_g}{C + C_g} \approx \frac{1}{2} \frac{C_g}{C}$. Now we can give the final result

$$H_C^x = \sum_{j=1}^{n} \frac{1}{2} \epsilon \sigma_j^z + g_C^x \sum_{j=1}^{n-1} \sigma_j^x \sigma_{j+1}^x, \tag{3.24}$$

with the coupling energy

$$g_C^x = \frac{1}{2}\lambda\epsilon = \frac{1}{4}\frac{C_g}{C}\epsilon. \tag{3.25}$$

So we have found another option the couple tunable transmons by their σ^x operators as we need it for our emulator of the Fermi-Hubbard model. The question now is which of the methods derived in this and the preceding section is superior and will subsequently be the choice for an experimental realization. This problem will be discussed in the following section.

3.1.3 Why Capacitances Are Preferable

To check which of the mentioned concepts for the σ^x-type interaction between tunable transmons should be preferred for the experimental realization, we investigate some of their potential problems.

We start by comparing the approximations we did during the derivation of the different coupling energies. For both methods we used the usual fixing of the high energy degree of freedom of the transmon, related to the small intrinsic inductance of the loop that contains the Josephson junctions, but this has proven not to cause problems for transmons, and would affect both methods likewise.

For the coupling via inductances, the only other approximation that followed was given in equation (3.7). However, in the text following that equation it is also argued how this should not produce much of an error. Even with deviations in the electrical elements—most likely in the Josephson junctions, as they are hard to consistently manufacture—and tuning of the transmons to the same energy through distinct external phases, when this term gives a finite value (due to the α_j^x now being different), it is always small compared to the diagonal qubit terms. The effect on the eigenstates is therefore negligible.

The main approximation in the case of capacitative coupling is more subtle. It lies in the transformation from the Lagrangian (3.20) to the Hamiltonian (3.21). If one resorts back to the mathematical excursus in section 3.1.2, checking equation (3.15), we see that if we would account for higher orders of λ, the Hamiltonian (3.21) would contain not only nearest neighbor interaction, but also an interaction that decays exponentially over the distance with λ^m towards the m^{th} neighbor qubit. Note that this decaying interaction cannot be mapped on a similar long range interaction between the fermions in the Fermi-Hubbard model; the Jordan-Wigner transformation would rather transform it into a complicated interaction of no physical meaning and is therefore unwanted. However, since λ is very small the approximation is very good. In fact λ could be adjusted such that terms of order $\mathcal{O}(\lambda^2)$ would already disappear in the unavoidable noise of the qubit system. One can either convince oneself numerically that the coefficients in front of these terms are quite well behaved and the approximation is valid, or look at the problem of inverting A_q from equation (3.11) in more detail in the full analytic solution for the

matrix elements in [19].

From these standpoints there are no advantages for either solution. One difference is however the coupling energy. As one can see in equation (3.8) and the following definition of g_j, for the coupling via inductances, the coupling strength is shifted relative to the qubit energy if the external phases are tuned; whereas equation (3.23) and the definition of $\tilde{g}_j$ show how in the case of capacitative coupling, the coupling energy always keeps the same ratio with the qubit energies. One could argue, that this might be an advantage for the first setup, as the coupling can be tuned relative to the qubit energy and therefore a range of different parameters for the emulation can be studied on one single chip, without changing electrical elements. But as it will turn out, the σ^z-type coupling will also be tunable, and the ratio of the couplings can be tuned even if the coupling strength of the coupling via capacitances stays the same relative to the qubit energy. For the emulator only the ratio of the different couplings is important as this determines the ratio of the parameters U and t in the Fermi-Hubbard Hamiltonian (2.27), and therefore determines the dynamics of the fermionic model. In fact, this matter turns out to be an advantage for the capacitive coupling: Since the coupling energy here scales with the qubit energies, if one considers deviations in the manufacturing of the transmons which are evened out through the external fluxes, the coupling strength between all qubits will be equal. If one couples via inductances this would also lead to deviations in the coupling energies because of the deviation in the separate fluxes, which does not resemble the Fermi-Hubbard model as we had intended.

Another important advantage of the coupling via capacitances is that it is much easier to build. One has to achieve only a small capacitance between neighboring qubits; this can be done by simply putting them closely next to each other on the chip. By putting them far apart, the coupling can be made as small as one wishes and theoretically, even very strong coupling could be achieved if one introduces extra finger capacitors, similar to those in the transmon qubits (see section 2.3). To obtain small coupling by inductances is on the other hand a problem: If one checks equation (3.10), and uses $\frac{E_C}{E_J} \approx \frac{1}{50}$ for transmons, one can see that E_{L_g} has to be of the order of the qubit energy to get small coupling, for example $\frac{g_C^x}{\epsilon} \approx \frac{1}{10}$. This means that the inductances L_g must be quite large. In fact, if one estimates the size of a circular loop with the inductance large enough to enter this limit, by using the formula $L_g \approx \mu_0 r \ln(\frac{8r}{d})$ [20], where r is the radius of the loop and d is the thickness of the wire, and plugging in $d \approx 100\,\text{nm}$, one can estimate a radius $r \approx 4\,\text{mm}$ for such a structure. This is a full order of magnitude larger than a transmon itself. One could optimize this by for example using zigzag lines, but still one ends up with a very large structure to implement on the chip. This would make a chip with many transmons unnecessarily large, and the size would make it more susceptible for noise.

This leads to the conclusion that the coupling via capacitances is the more viable option to realize our σ^x-type coupling between transmons and will therefore be the method we will use in the following. However, before we discuss the complete circuit of the emulator, we will have to address first how we intent to implement the σ^z coupling.

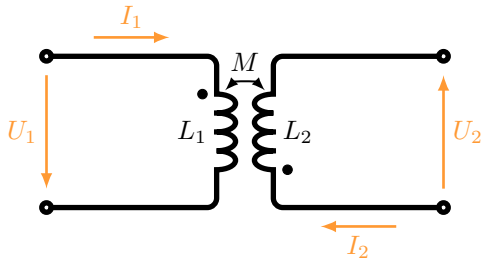

Figure 3.3: Circuit diagram of two inductances L_1 and L_2 forming a mutual inductance $M = k_M\sqrt{L_1 L_2}$ with $k_M \in (0,1)$. U_1 is the voltage across the left inductance, I_1 the current through it. U_2 and I_2 are voltage across and current through the right inductance. The dots beside the inductances indicate a sign convention, which describes in which direction parts of the induced magnetic flux of one inductance enter the other one and vice versa.

3.2 Coupling of Tunable Transmons via σ^z

To address how our emulator should incorporate the on-site terms of the Fermi-Hubbard model, we saw in figure 2.4 of section 2.4.2 that we need to couple tunable transmons by their σ^z operators. This requires nonlinear coupling between the phases of the transmons which is not a trivial task to perform; a method how to achieve this had to be invented.

The idea behind this method comes from the mechanism how the transmon is tuned, as described in section 2.3: The external tuning field couples to the cosine potential of the qubit's degree of freedom through the phase difference across the small inductance of the loop containing the Josephson junctions. The degree of freedom of this phase difference was ignored because its excitation energy is much larger than the energy splitting of the qubit. However, we hoped that by coupling the inductances of two transmons to form a mutual inductance, which means coupling these previously ignored degrees of freedom, the desired nonlinear interaction would arise.

This section shows that this mechanism in fact does give the correct σ^z-type interaction between the transmons and derives in detail how it works.

3.2.1 Coupled Inductances

In order to calculate the coupling of two transmons by their inductances, we start by deriving how to treat a mutual inductance in the context of quantum circuits, which means deriving the energy term to insert into the Lagrangian of a system containing coupled inductances.

For this, consider two inductances L_1 and L_2 coupled together to form a mutual inductance M as shown in figure 3.3. In general, it holds that

$$M = k_M\sqrt{L_1 L_2} \tag{3.26}$$

with $k_M \in (0,1)$, and for the voltage U_1 across and the current I_1 through the first

inductance and respectively U_2 and I_2 for the second one we have

$$\begin{aligned} U_1 &= L_1\dot{I}_1 + M\dot{I}_2, \\ U_2 &= L_2\dot{I}_2 + M\dot{I}_1. \end{aligned} \tag{3.27}$$

The plus sign in front of the terms with M stems from the sign convention used in figure 3.3. If both currents enter (or both leave) the inductance at the dot, the sign is a plus; it is a minus sign otherwise. The origin of this is in which direction, due to the geometry of the setup, parts of the induced flux in one inductance enter the other inductance and vice versa; think of two coils in a transformer and regard how they can be winded in different directions.

Now we look at the energy V_M of this system, which can quickly be derived to be

$$\begin{aligned} V_M &= \int (U_1 I_1 + U_2 I_2)\, \mathrm{d}t \\ &= \int \left(L_1\dot{I}_1 I_1 + L_2\dot{I}_2 I_2 + M(\dot{I}_1 I_2 + \dot{I}_2 I_1)\right) \mathrm{d}t \\ &= \frac{1}{2}L_1 I_1^2 + \frac{1}{2}L_2 I_2^2 + M I_1 I_2, \end{aligned} \tag{3.28}$$

where we—for the moment—ignore constants of integration. To use this in the context of superconducting circuits we want to change our variables from currents to fluxes (and eventually phases). Using the laws of electromagnetic induction, we can write voltage as time derivative of magnetic flux $U_{(1,2)} = -\dot{\Phi}_{(1,2)}$, so by integrating equations (3.27) we find

$$\begin{aligned} -(\Phi_1 - \Phi_{10}) &= L_1 I_1 + M I_2, \\ -(\Phi_2 - \Phi_{20}) &= L_2 I_2 + M I_1, \end{aligned} \tag{3.29}$$

where we introduced Φ_{10} and Φ_{20} as the constants of integration. They can be interpreted as constant external magnetic fluxes through each of the inductances and are important, as seen in section 2.3, since they will end up to be the tool to tune our transmons. Let us for the moment introduce $\Phi'_{(1,2)} = \Phi_{(1,2)} - \Phi_{(1,2)0}$ as a convenient notation. We can then rewrite the upper expressions as

$$\begin{aligned} I_1 &= -\frac{1}{L_1 - \frac{M^2}{L_2}}\left(\Phi'_1 - \frac{M}{L_2}\Phi'_2\right) \\ &= -\frac{1}{1-k_M^2}\frac{1}{L_1}\left(\Phi'_1 - k_M\sqrt{\frac{L_1}{L_2}}\Phi'_2\right), \\ I_2 &= -\frac{1}{1-k_M^2}\frac{1}{L_2}\left(\Phi'_2 - k_M\sqrt{\frac{L_2}{L_1}}\Phi'_1\right). \end{aligned} \tag{3.30}$$

Inserting this in V_M from equation (3.28) gives

$$\begin{aligned} V_M &= \Big(\frac{1}{1-k_M^2}\Big)^2\Big(\frac{1}{2L_1}\Big(\Phi_1' - k_M\sqrt{\frac{L_1}{L_2}}\Phi_2'\Big)^2 + \frac{1}{2L_2}\Big(\Phi_2' - k_M\sqrt{\frac{L_2}{L_1}}\Phi_1'\Big)^2 \\ &\quad - \frac{k_M}{\sqrt{L_1L_2}}\Big(\Phi_1' - k_M\sqrt{\frac{L_1}{L_2}}\Phi_2'\Big)\Big(\Phi_2' - k_M\sqrt{\frac{L_2}{L_1}}\Phi_1'\Big)\Big) \\ &= \frac{1}{1-k_M^2}\Big(\frac{1}{2L_1}\Phi'^2_1 + \frac{1}{2L_2}\Phi'^2_2 - \frac{k_M}{\sqrt{L_1L_2}}\Phi'_1\Phi'_2\Big). \end{aligned} \tag{3.31}$$

Finally, let us convert this expression into the form used in superconducting circuits by introducing the phases $\phi_{(1,2)} = \frac{2e}{\hbar}\Phi_{(1,2)}$ across the inductances and $\phi_{(1,2)0} = \frac{2e}{\hbar}\Phi_{(1,2)0}$ for the external fluxes. This gives the result

$$\begin{aligned} V_M &= \Big(\frac{\hbar}{2e}\Big)^2\frac{1}{1-k_M^2}\Big(\frac{1}{2L_1}(\phi_1-\phi_{10})^2 + \frac{1}{2L_2}(\phi_2-\phi_{20})^2\Big) \\ &\quad - \Big(\frac{\hbar}{2e}\Big)^2\frac{k_M}{1-k_M^2}\frac{1}{\sqrt{L_1L_2}}(\phi_1-\phi_{10})(\phi_2-\phi_{20}). \end{aligned} \tag{3.32}$$

This result could have also been derived from a generalized form given in the section of the inductive coupling of flux qubits in the paper from Wendin and Shumeiko [8]. However, the derivation here gave a clearer insight where this result stems from.

Two Identical Inductances

A special case to consider is when the two inductances are equal, i. e. $L_1 = L_2 = L$. This will be important later, since we want to inductively couple two identical transmons. Equation (3.31) can then be written as

$$\begin{aligned} V_M &= \frac{1}{1-k_M^2}\frac{1}{2L}\big((\Phi_1' - \Phi_2')^2 + 2(1-k_M)\Phi_1'\Phi_2'\big) \\ &= \frac{1}{1-k_M^2}\frac{1}{2L}(\Phi_1' - \Phi_2')^2 + \frac{1}{1+k_M}\frac{1}{L}\Phi_1'\Phi_2'. \end{aligned} \tag{3.33}$$

As a side note, it is interesting at this point to check for the limits for k_M. One can see how $k_M \to 0$ will of course eliminate the coupling and the total energy will be the sum of the energies of the individual inductances. For $k_M \to 1$, since the energy should not diverge (which means $V \nrightarrow \infty$), as a consequence both fluxes will attain the same value as $\Phi_1' - \Phi_2'$ has to go to zero; this limit of close coupling is indeed familiar from transformers.

For the last step here, we will also rewrite this expression using phases and obtain

$$\begin{aligned} V_M &= \Big(\frac{\hbar}{2e}\Big)^2\frac{1}{1-k_M^2}\frac{1}{2L}\big((\phi_1-\phi_{10}) - (\phi_2-\phi_{20})\big)^2 \\ &\quad + \Big(\frac{\hbar}{2e}\Big)^2\frac{1}{1+k_M}\frac{1}{L}(\phi_1-\phi_{10})(\phi_2-\phi_{20}). \end{aligned} \tag{3.34}$$

We will use this form to derive how this inductive coupling mechanism acts on transmons.

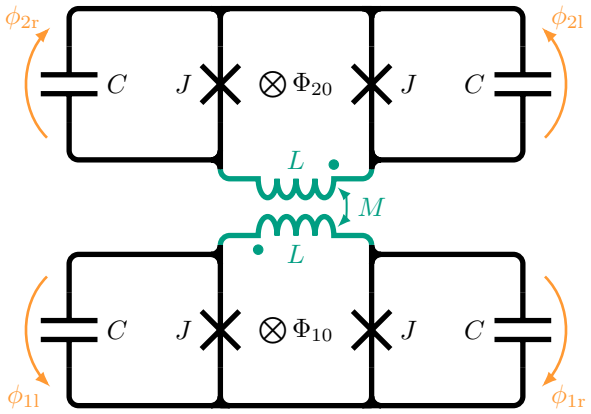

Figure 3.4: Circuit diagram of two inductively coupled transmons, where their inductances L form a mutual inductance $M = k_M L$ with $k_M \in (0,1)$. The transmons are considered to be build identically with Josephson junctions J and shunt capacities C, but with different external fluxes Φ_{10} and Φ_{20} for tuning. $\phi_{(1,2)\mathrm{l}}$ and $\phi_{(1,2)\mathrm{r}}$ denote the phase differences across the junctions. This setup gives a σ^z-type interaction between the tunable transmons. The coupling strength is $g^z = -\frac{k_M}{16}\tan(\frac{\phi_{10}}{2})\tan(\frac{\phi_{20}}{2})\frac{\epsilon_1\epsilon_2}{E_L}$, where $\epsilon_{(1,2)}$ are the qubit energies, and $\phi_{(1,2)0} = \frac{2e}{\hbar}\Phi_{(1,2)0}$ as well as $E_L = (\frac{\hbar}{e})^2\frac{1}{L}$; the coupling strength can therefore be tuned by the external fields, also its sign can be changed.

3.2.2 Two Tunable Transmons Coupled by a Mutual Inductance

Now that we know how to treat a mutual inductance in our circuit, we will analyse the situation of inductively coupled transmons. For this, consider two transmons with capacitances C, Josephson junctions J with critical current I_c, and their inductances L forming a mutual inductance $M = k_M L$ ($k_M \in (0,1)$), with the phases across the junctions of the two transmons being denoted $\phi_{(1,2)\mathrm{l}}$ and $\phi_{(1,2)\mathrm{r}}$ as shown in figure 3.4. For the external magnetic fluxes $\Phi_{(1,2)0}$ we introduce the phases $\phi_{(1,2)0} = \frac{2e}{\hbar}\Phi_{(1,2)0}$. The Lagrangian of this setup reads (using figure 2.2 of section 2.2.1 and equation (3.34) from above):

$$\begin{aligned}\mathcal{L}^z = &\left(\frac{\hbar}{2e}\right)^2\frac{1}{2}C(\dot{\phi}_{1\mathrm{l}}^2 + \dot{\phi}_{1\mathrm{r}}^2 + \dot{\phi}_{2\mathrm{l}}^2 + \dot{\phi}_{2\mathrm{r}}^2)\\ &+ \frac{\hbar}{2e}I_c(\cos(\phi_{1\mathrm{l}}) + \cos(\phi_{1\mathrm{r}}) + \cos(\phi_{2\mathrm{l}}) + \cos(\phi_{2\mathrm{r}}))\\ &- \left(\frac{\hbar}{2e}\right)^2\frac{1}{2L}\frac{1}{1-k_M^2}\big((\phi_{1\mathrm{l}} - \phi_{1\mathrm{r}} - \phi_{10}) - (\phi_{2\mathrm{l}} - \phi_{2\mathrm{r}} - \phi_{20})\big)^2\\ &- \left(\frac{\hbar}{2e}\right)^2\frac{1}{2L}\frac{2}{1+k_M}(\phi_{1\mathrm{l}} - \phi_{1\mathrm{r}} - \phi_{10})(\phi_{2\mathrm{l}} - \phi_{2\mathrm{r}} - \phi_{20}).\end{aligned} \tag{3.35}$$

Defining $\phi_{(1,2)} := \frac{1}{2}(\phi_{(1,2)\mathrm{l}} + \phi_{(1,2)\mathrm{r}})$ and $\phi_\pm := \frac{1}{2}((\frac{\phi_{1\mathrm{l}}-\phi_{1\mathrm{r}}}{2} - \frac{\phi_{10}}{2}) \pm (\frac{\phi_{2\mathrm{l}}-\phi_{2\mathrm{r}}}{2} - \frac{\phi_{20}}{2}))$, using that the external fields are constant, meaning $\dot{\phi}_{(1,2)0} = 0$, and using the addition theorem $\cos(\phi_{(1,2)\mathrm{l}}) + \cos(\phi_{(1,2)\mathrm{r}}) = 2\cos(\frac{\phi_{(1,2)\mathrm{l}}+\phi_{(1,2)\mathrm{r}}}{2})\cos(\frac{\phi_{(1,2)\mathrm{l}}-\phi_{(1,2)\mathrm{r}}}{2})$ for the cosine

terms one can rewrite

$$\begin{aligned}\mathcal{L}^z = &\Big(\frac{\hbar}{2e}\Big)^2 C(\dot\phi_1^2 + \dot\phi_2^2 + 2\dot\phi_+^2 + 2\dot\phi_-^2)\\ &+ \frac{\hbar}{e} I_c(\cos(\phi_1)\cos(\frac{\phi_{10}}{2} + \phi_+ + \phi_-) + \cos(\phi_2)\cos(\frac{\phi_{20}}{2} + \phi_+ - \phi_-))\\ &- \Big(\frac{\hbar}{2e}\Big)^2 \frac{2}{L}\Big(\frac{4}{1-k_M^2} - \frac{2}{1+k_M}\Big)\phi_-^2 - \Big(\frac{\hbar}{2e}\Big)^2 \frac{2}{L}\frac{2}{1+k_M}\phi_+^2. \end{aligned} \tag{3.36}$$

Introducing $N_{(1,2,\pm)} = \frac{1}{\hbar}\frac{\partial \mathcal{L}^z}{\partial \dot\phi_{(1,2,\pm)}}$, defining the energies $E_C = \frac{e^2}{C}$, $E_J = \frac{\hbar}{e} I_c$ as well as $E_L = (\frac{\hbar}{e})^2 \frac{1}{L}$, furthermore defining $\xi_+ = \frac{2}{1+k_M}$ and $\xi_- = \frac{4}{1-k_M^2} - \frac{2}{1+k_M}$ allows us to express the corresponding Hamiltonian by

$$\begin{aligned}H^z = &E_C(N_1^2 + N_2^2 + \frac{1}{2}N_+^2 + \frac{1}{2}N_-^2) + \frac{1}{2}E_L\xi_+\phi_+^2 + \frac{1}{2}E_L\xi_-\phi_-^2\\ &- E_J\cos(\phi_1)\cos(\frac{\phi_{10}}{2} + \phi_+ + \phi_-) - E_J\cos(\phi_2)\cos(\frac{\phi_{20}}{2} + \phi_+ - \phi_-). \end{aligned} \tag{3.37}$$

Recalling that L is very small, we find E_L to be very large (compared to E_J). We can therefore ignore terms proportional to $E_J\phi_\pm^2$ towards those proportional to $E_L\phi_\pm^2$, which justifies expanding the cosines for small $\phi_\pm$ giving

$$\begin{aligned}H^z = &E_C(N_1^2 + N_2^2 + \frac{1}{2}N_+^2 + \frac{1}{2}N_-^2) + \frac{1}{2}E_L\xi_+\phi_+^2 + \frac{1}{2}E_L\xi_-\phi_-^2\\ &- E_J\cos(\phi_1)\big(\cos(\frac{\phi_{10}}{2}) - \sin(\frac{\phi_{10}}{2})(\phi_+ + \phi_-)\big)\\ &- E_J\cos(\phi_2)\big(\cos(\frac{\phi_{20}}{2}) - \sin(\frac{\phi_{20}}{2})(\phi_+ - \phi_-)\big). \end{aligned} \tag{3.38}$$

We can now identify the qubit energy terms $E_C N_{(1,2)}^2 - E_J\cos(\frac{\phi_{(1,2)0}}{2})\cos(\phi_{(1,2)}) = \frac{1}{2}\epsilon_{(1,2)}\sigma_{(1,2)}^z$ (see equation (2.15)), also harmonic oscillators $\frac{1}{2}E_C N_\pm^2 + \frac{1}{2}E_L\xi_\pm\phi_\pm^2 = \hbar\omega_\pm(a_\pm^\dagger a_\pm + \frac{1}{2})$ with $\omega_\pm = \frac{1}{\hbar}\sqrt{\xi_\pm E_C E_L}$ and therefore $\phi_\pm = \frac{1}{\sqrt{2}}(\frac{E_C}{\xi_\pm E_L})^{\frac{1}{4}}(a_\pm^\dagger + a_\pm)$. We know that $\cos(\phi_{(1,2)})$ are diagonal in the qubit basis (see equation (2.19)), hence $\cos(\phi_{(1,2)}) = \alpha_{(1,2)}^z\sigma_{(1,2)}^z + \beta_{(1,2)}\mathbb{1}$. Following the above argument that ϕ is very small, we neglect terms proportional to $E_J\mathbb{1}\phi \approx 0$ and also leave out constant terms, resulting in

$$\begin{aligned}H^z = &\frac{1}{2}\epsilon_1\sigma_1^z + \frac{1}{2}\epsilon_2\sigma_2^z + \hbar\omega_+ a_+^\dagger a_+ + \hbar\omega_- a_-^\dagger a_-\\ &+ (g_{1+}\sigma_1^z + g_{2+}\sigma_2^z)(a_+^\dagger + a_+) + (g_{1-}\sigma_1^z - g_{2-}\sigma_2^z)(a_-^\dagger + a_-), \end{aligned} \tag{3.39}$$

with $g_{(1,2)\pm} = E_J\alpha_{(1,2)}^z\sin(\frac{\phi_{(1,2)0}}{2})\frac{1}{\sqrt{2}}(\frac{E_C}{\xi_\pm E_L})^{\frac{1}{4}}$.

For the next step, take the displacement operators $D_\pm(d) = \mathrm{e}^{da_\pm^\dagger - d^\dagger a_\pm}$, for any operator d with $[d, a_\pm] = [d, a_\pm^\dagger] = [d, d^\dagger] = 0$. With the Baker–Campbell–Hausdorff formula and its related Hadamard lemma one can check that the displacement operators are unitary and it holds that $D_\pm^\dagger(d)a_\pm D_\pm(d) = a_\pm + d$ and $D_\pm^\dagger(d)a_\pm^\dagger D_\pm(d) = a_\pm^\dagger + d^\dagger$, as well as $D_\pm^\dagger(d)a_\pm^\dagger a_\pm D_\pm(d) = a_\pm^\dagger a_\pm + d^\dagger a_\pm + d a_\pm^\dagger + d^\dagger d$. We continue by defining the

unitary operator

$$U = D_+(-\frac{1}{\hbar\omega_+}(g_{1+}\sigma_1^z + g_{2+}\sigma_2^z))D_-(-\frac{1}{\hbar\omega_-}(g_{1-}\sigma_1^z - g_{2-}\sigma_2^z)) \tag{3.40}$$

and by again neglecting constant terms the Hamiltonian transforms to

$$U^\dagger H^z U = \frac{1}{2}\epsilon_1\sigma_1^z + \frac{1}{2}\epsilon_2\sigma_2^z + \hbar\omega_+ a_+^\dagger a_+ + \hbar\omega_- a_-^\dagger a_- + g_z\sigma_1^z\sigma_2^z, \tag{3.41}$$

with $g^z = -2(\frac{g_{1+}g_{2+}}{\hbar\omega_+} - \frac{g_{1-}g_{2-}}{\hbar\omega_-})$. Because of the small inductance of the transmons, the energy $\hbar\omega_\pm$ is very big compared to the qubit energies such that the oscillators' excitation can be ignored again; they are just needed to mediate an effective interaction between the qubits.

Let us further analyze the coupling energy g^z. We start by pulling the dependence on $\xi_\pm$ out of the coefficients by introducing $g_{(1,2)} = E_J\alpha^z_{(1,2)}\sin(\frac{\phi_{(1,2)0}}{2})\frac{1}{\sqrt{2}}(\frac{E_C}{E_L})^{\frac{1}{4}}$ and $\omega = \frac{1}{\hbar}\sqrt{E_C E_L}$, such that $g_{(1,2)\pm} = (\frac{1}{\xi_\pm})^{\frac{1}{4}}g_{(1,2)}$ and $\omega_\pm = \sqrt{\xi_\pm}\omega$. This gives

$$g^z = -2(\frac{1}{\xi_+} - \frac{1}{\xi_-})\frac{g_1 g_2}{\hbar\omega} = -2k_M\frac{g_1 g_2}{\hbar\omega}, \tag{3.42}$$

where we used the convenient identity $(\frac{1}{\xi_+} - \frac{1}{\xi_-}) = k_M$. Using the equations (2.16) and (2.19) we have

$$\epsilon_{(1,2)} = \sqrt{2E_C E_J\cos(\frac{\phi_{(1,2)0}}{2})}, \text{ and } \alpha^z_{(1,2)} = -\frac{1}{4}\sqrt{\frac{2E_C}{E_J\cos(\frac{\phi_{(1,2)0}}{2})}} \tag{3.43}$$

and one can check that for our effective Hamiltonian

$$H^z_{\text{eff}} = \frac{1}{2}\epsilon_1\sigma_1^z + \frac{1}{2}\epsilon_2\sigma_2^z + g_z\sigma_1^z\sigma_2^z, \tag{3.44}$$

it holds that

$$g^z = -\frac{k_M}{16}\tan(\frac{\phi_{10}}{2})\tan(\frac{\phi_{20}}{2})\frac{\epsilon_1\epsilon_2}{E_L}. \tag{3.45}$$

This is a beautiful result regarding the linear dependence on the coupling parameter $k_M \in (0,1)$ of the mutual inductance; respectively it is linear in the mutual inductance, i. e., $g^z \propto M$ since $\frac{1}{E_L} \propto L$ and $M = k_M L$. Furthermore, the coupling strength g^z is comfortably tunable through the external fields applied in the transmons. Also its sign can be changed by inverting one of the fluxes, which would give the possibility to emulate a Fermi-Hubbard model with repulsive or attractive on-site energies. One remaining issue is still that E_L is big compared to the qubit energies. This causes the coupling to be very small in comparison to the qubit energies; and therefore the consequences need to be investigated, which will be done in the following sections 3.3.2 and 3.3.3.

Another issue which we will quickly address at this point is if and how our unitary

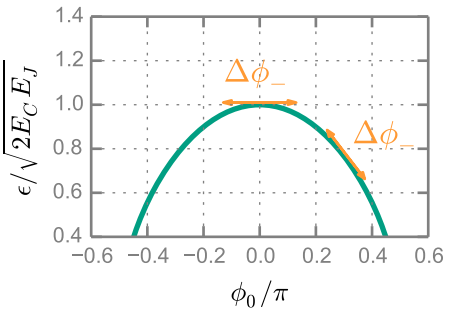

Figure 3.5: The transmon energy ϵ (normalized by its maximum value) over the phase ϕ_0 of the external tuning flux. Variations in the phase difference ϕ_- across the loop inductance of a transmon cause the qubit energy to vary as well. This effect is stronger for larger absolute values of ϕ_0 due to a steeper slope.

transformation (3.41) changes our observables. We can however immediately see, that $U^\dagger \sigma^z_{(1,2)} U = \sigma^z_{(1,2)}$, so the measurements of $\sigma^z_{(1,2)}$—and therefore the measurements whether our emulated fermions are excited or not—are not affected. With our emulator in mind we also need to assume our qubits to be coupled via $\sigma^x_{(1,2)}$ to additional qubits. Using the Baker–Campbell–Hausdorff formula, respectively its related Hadamard lemma and the commutation relations of the Pauli operators, we can easily check that it holds that $\mathrm{e}^{\theta\sigma^z}\sigma^x\mathrm{e}^{-\theta\sigma^z} = \cos(\theta)\sigma^x + \sin(\theta)\sigma^y = \mathrm{e}^{-\mathrm{i}\theta}\sigma^+ + \mathrm{e}^{\mathrm{i}\theta}\sigma^-$. With this, one can see that $U^\dagger\sigma^x_{(1,2)}U = \mathrm{e}^{-\mathrm{i}\theta_{(1,2)}}\sigma^+_{(1,2)} + \mathrm{e}^{\mathrm{i}\theta_{(1,2)}}\sigma^-_{(1,2)}$, where $\theta_{(1,2)} = -\frac{g_{(1,2)}}{\hbar\omega_+}(a_+^\dagger - a_+) - \frac{g_{(1,2)}}{\hbar\omega_-}(a_-^\dagger - a_-)$. So one the one hand, $\theta_{(1,2)}$ will be very small since the fraction $\frac{g_{(1,2)}}{\hbar\omega_\pm}$ is small itself and the expectation value of $a_\pm^\dagger - a_\pm$ is also small if the oscillators are unlikely to be excited; which means the transformation barely changes the operator. On the other hand it would be in any case irrelevant: Interactions would in our case transform like $\sigma_1^x\sigma_2^x \sim \sigma_1^+\sigma_2^- + \sigma_2^+\sigma_1^- \mapsto \mathrm{e}^{\mathrm{i}(\theta_2-\theta_1)}\sigma_1^+\sigma_2^- + \mathrm{h.c.}$, so the transformation only contributes a phase factor of no physical relevance.

We have found that we can couple transmons by their σ^z operators by coupling the inductances of their loops containing the Josephson junctions to form a mutual inductance. This creates a coupling of the degrees of freedom associated with the phase differences across the inductances. These degrees of freedom have since been ignored due to the high energy that is needed to excite them (see section 2.3). Because these degrees of freedom couple to the cosine potential of the low energy degree of freedom of the transmon that gives the qubit states, we were able to show that the previously ignored degrees of freedom therefore mediate an effective interaction between the σ^z operators of the transmons. Figure 3.5 helps explaining this with a picture: We plotted the qubit energy ϵ over the phase ϕ_0 of the external tuning flux. Variations in the phase difference ϕ_- across the loop inductance vary the qubit energy. Because of the steeper slope for large absolute values of ϕ_0, variations in ϕ_- have a larger impact, which explains the dependence of the coupling energy of the σ^z coupling on ϕ_0 in equation (3.45).

Having clarified this issue, we can continue with the full circuit for our emulator and study the tunability as well as the range of validity of it, especially concerning the indicated problem of very small coupling strengths for our σ^z-type coupling.

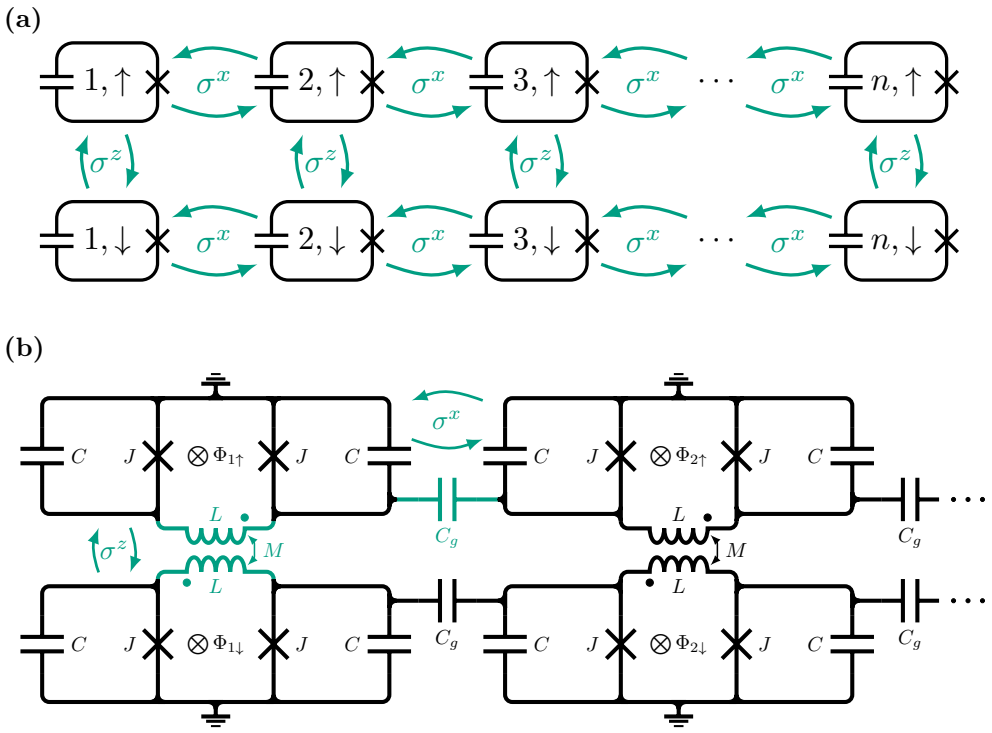

Figure 3.6: **(a)** The sketch of figure 2.4 in section 2.4.2. It shows the fundamental design for an emulator of the Fermi-Hubbard model in one dimension. The system of $2n$ qubits coupled by their σ^z and σ^x operators in the pictured fashion has a Hamiltonian that is equivalent to the Fermi-Hubbard Hamiltonian. **(b)** The circuit diagram for a realization of a qubit system in accordance with the upper sketch based on tunable transmon qubits. The coupling through capacitances C_g provides the σ^x-type interactions, coupling the inductances of the transmons to form a mutual inductances M leads to interactions via σ^z.

3.3 The Full Circuit of the Emulator

This section will summarize our findings up to this point, as we are now able to give the full circuit diagram of a superconducting circuit based on transmon qubits, that works as an emulator for the Fermi-Hubbard model in one dimension. This means the circuit has an equivalent Hamiltonian to this model and we can give the quantities corresponding to the parameters U and t of the Fermi-Hubbard Hamiltonian (2.27) based on the values of the electrical elements and applied external magnetic fields in the circuit.

There will also be a brief comment on the tunability of the circuit through the external fields and on the experimental realization; how the circuit elements could look like implemented on a chip. We check that the emulator can actually be realized in the regime of parameters which is experimentally acquirable, and that our findings are not purely academic.

3.3.1 Summary of the Findings and Circuit Diagram

Let us first condense what has been achieved so far in the last two chapters, since we can now draw the full circuit for our emulator, which is a major result of this thesis. Figure 3.6 gives a good overview for this:

In figure 3.6 (a), we remind ourselves about the findings of chapter 2, and mainly section 2.4.2: A system of two chains of n qubits coupled by their σ^x operators, with the chains lined up next to each other such that opposite qubits are coupled by σ^z, gives a qubit system with the Hamiltonian

$$H_{\mathrm{E}} = \sum_{j=1}^{n} \sum_{s=\uparrow,\downarrow} \frac{1}{2} \epsilon \sigma_{j,s}^{z} + g^{z} \sum_{j=1}^{n} \sigma_{j,\uparrow}^{z} \sigma_{j,\downarrow}^{z} + g^{x} \sum_{j=1}^{n-1} \sum_{s=\uparrow,\downarrow} \sigma_{j,s}^{x} \sigma_{j+1,s}^{x}, \tag{3.46}$$

from equation (2.32) that is equivalent to the one-dimensional Fermi-Hubbard Hamiltonian

$$H_{\mathrm{FH}} = U \sum_{j=1}^{n} c_{j,\uparrow}^{\dagger} c_{j,\uparrow} c_{j,\downarrow}^{\dagger} c_{j,\downarrow} - t \sum_{j=1}^{n-1} \sum_{s=\uparrow,\downarrow} (c_{j,s}^{\dagger} c_{j+1,s} + c_{j+1,s}^{\dagger} c_{j,s}), \tag{3.47}$$

from equation (2.27).

Figure 3.6 (b) then encapsulates the outcomes of the calculations of this chapter. We have found methods to realize the two different kinds of couplings needed for the emulator, and are therefore able to give the full circuit diagram of a superconducting circuit based on transmons, that forms an emulator for the Fermi-Hubbard model. Two chains of transmons are coupled by capacitances to give—as section 3.1.2 shows—the σ^x-type interacting of the sketch in figure 3.6 (a). Section 3.2.2 derived, that the coupling of two opposite transmons by a mutual inductance, formed by the inductances of their loops, gives the coupling via σ^z.

The preceding sections also gave formulas for the coupling energies depending on the electrical elements in the circuit in figure 3.6. We combine the equations (2.33), (3.45) and (3.25), such that we can determine the parameters for the emulated Fermi-Hubbard model to be

$$U = 4g^{z} = \pm \frac{1}{4} \tan^{2}\left(\frac{\phi_0}{2}\right) \frac{\epsilon^2}{E_M} \tag{3.48}$$

and

$$t = -g^{x} = -\frac{1}{4} \frac{C_g}{C} \epsilon, \tag{3.49}$$

with the energy splitting ϵ of all qubits and the energy $E_M = (\frac{\hbar}{e})^2 \frac{1}{M}$ associated with the mutual inductance M. We set the external fluxes to the values $\Phi_{j\uparrow} = \frac{\hbar}{2e}\phi_0$ and $\Phi_{j\downarrow} = \mp\Phi_{j\uparrow}$, where a sign change here causes the sign change in the upper equation (3.48).

We have now established the circuit and quantities of our emulator; let us continue by exploring it in more detail.

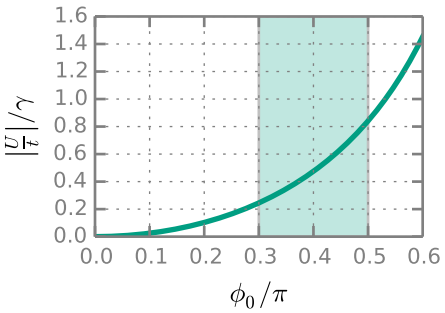

Figure 3.7: Plot of the fraction $\frac{U}{t}$ of the parameters of the Fermi-Hubbard model the emulator is equivalent to over the phase ϕ_0 associated with the external tuning flux. The plot shows the tunability of the properties of the emulated system by external quantities. Because of noise effects, the range for ϕ_0 is experimentally limited. The approximate range for ϕ_0 that is reasonable is shaded in light green. We can therefore see that we are able to tune $\frac{U}{t}$ by quite a large factor.

3.3.2 Tunability

An important feature of the circuit in figure 3.6 (b) is tunability: If one is interested in the properties of the Fermi-Hubbard model, one would certainly care to investigate the effect of different parameter regimes of on-site energy U and transfer energy t. It would then be unfavorable to be forced to manufacture a specific chip for each set of parameters one would like to observe. Being able to tune the parameters of the emulator through external signals, using just one single chip is therefore a great advantage. Many measurements could then be performed on this single chip, which has the benefit of not having to cool down the system below 20 mK after switching chips; this greatly speeds up the process of multiple measurements for different parameters. Moreover, producing a single ship is faster and less expensive than producing multiple chips.

As we can determine from equations (3.48) and (3.49), in our case the fraction $\frac{U}{t}$ is indeed tunable via the external phase ϕ_0 related to the external magnetic fluxes through the tunable transmons. We find our ratio to be

$$\left|\frac{U}{t}\right| = \gamma\sqrt{\cos(\frac{\phi_0}{2})}\tan^2(\frac{\phi_0}{2}), \tag{3.50}$$

with the constant scale factor $\gamma = \frac{C}{C_g}\frac{\hat{\epsilon}}{E_M}$, where we separated the dependence of the qubit energies ϵ (see equation (2.16)) on the external phase, such that $\epsilon = \hat{\epsilon}\sqrt{\cos(\phi_0/2)}$, with the constant $\hat{\epsilon}$. In figure 3.7, $|\frac{U}{t}|$ is plotted against ϕ_0 to give an insight into our options of tunability. Within a reasonable range of ϕ_0 up to around $\frac{\pi}{4}$, we can observe quite a large factor between the lower and upper limit for the ratio of the parameters. The lower limit is due to the fact that for too small absolute values of U, it will be of the order of the energy scale related to noise; we would not get meaningful emulation results in this regime. The upper limit is also related to this, as larger external phases also increase the transmons susceptibility to noise. This problem will be analyzed in more detail in the following section 3.3.3.

Another feature is available through external tuning: If we use different phases for

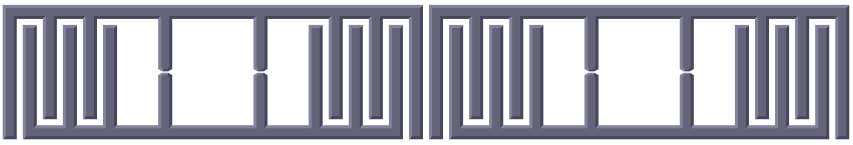

Figure 3.8: Sketch of two tunable transmons being placed side by side. This leads to a capacitance between the qubits that is small compared to the shunt capacities, yet causes a weak but perceivable σ^x-type coupling between the transmons.

the external fluxes through each of the two chains, denoting them $\phi_{0\uparrow}$ and $\phi_{0\downarrow}$, we can write the on-site energy (see equations (3.45)) as

$$U = \tilde{\gamma}\sqrt{\cos(\frac{\phi_{0\uparrow}}{2})\cos(\frac{\phi_{0\downarrow}}{2})}\tan(\frac{\phi_{0\uparrow}}{2})\tan(\frac{\phi_{0\downarrow}}{2}), \tag{3.51}$$

with the constant $\tilde{\gamma} = -\frac{1}{4}\frac{\hat{\epsilon}^2}{E_M}$. Therefore the sign of U can be switched, depending on the external fluxes going in the same or in the opposite direction. This means we can, on the same ship, emulate the Fermi-Hubbard model with repulsive or attractive on-site interaction.

The precise range of parameter regimes that may be emulated has to be determined, if one is at the point of having a concrete circuit layout in an experiment. The question that will be addressed next is whether or not an emulator, that gives meaningful results, could be build at the current state of technology.

3.3.3 Remarks on an Experimental Realization

The discussion in section 3.1.3 already mentioned how one could realize the σ^x interaction via coupling capacitances on a chip: The coupling energy scales with the capacitance between the qubits (see equation (3.49)). One can simply place the transmons close to each other as sketched in figure 3.8. This method can provide a coupling that is small enough such that the approximations in sections 2.4.2 and 3.1.2 are valid, yet is still well above noise level. This method for capacitative coupling is also commonly used for the initialization process which involves capacitative coupling of qubits to a transmission line resonator, which will be described in section 4.1.2, and has also been already demonstrated for coupling between qubits. In principle, virtually every coupling energy can be acquired: Starting from very small energies by placing the transmons further apart, up to strong coupling energies by adding extra finger capacitors between the transmons.

Unfortunately, the realization of the σ^z interaction of transmons is much more difficult. The problem lies in the coupling energy of the interaction: Resorting to section 3.2.2, the interaction between the qubits is mediated through additional degrees of freedom. The result is that the coupling energy is relatively small. To be precise on the matter what relatively small means, let us assume the transmons to have a moderate decoherence time of $T_2^* = 1\,\mu s$. Associated with this energy scale is therefore an energy scale with the corresponding frequency of 1 MHz. We have to compare the coupling

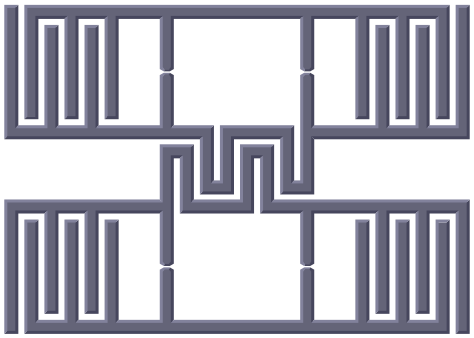

Figure 3.9: Sketch of two tunable transmons with increased loop inductance through a zigzag form of the wire to lengthen it. The opposite qubits match each others pattern, such that the inductances couple closely forming an as large as possible mutual inductance for the desired σ^z-type interaction between the transmons. An also emerging coupling via σ^x due to a capacitance among the qubits can be suppressed by tuning them to different energies, such that transitions through this interaction would violate energy conservation.

strength with this energy scale, where the coupling should be at least of the order of 10 MHz. Otherwise, the emulator does not to have time to let the dynamic of the system evolve, until decoherence destroys the quantum state in the emulator and therefore averts a meaningful result for the emulation.

Let us estimate roughly if this regime is accessible. For the dynamic of the emulator, U is the crucial quantity to look at. Referring to equation (3.48), we can express the magnitude of the on-site energy as $|U| = \frac{1}{4}\tan^2(\frac{\phi_0}{2})\frac{\epsilon^2}{E_M}$. We check the range for the external phase ϕ_0 first. Naively one could think $|U|$ can be arbitrarily large, since it diverges for $\phi_0 \to \pi$. However ϕ_0 is limited for mainly two reasons: Because the qubit energy $\epsilon = \sqrt{2E_C E_J \cos(\phi_0/2)}$ is increasingly sensitive to fluctuations of ϕ_0 for larger values of ϕ_0 (see the slope of ϵ in figure 3.5), increasing ϕ_0 will cause the energy splitting to fluctuate stronger, which results in stronger noise. Also if one assumes noise sources that capacitively couple to the transmon, one can derive analogously to equations (3.25) and (4.25), that the coupling strength scales with $\sqrt{\epsilon}$; relative to the qubit energy it therefore scales with $\frac{1}{\sqrt{\epsilon}}$. Increasing ϕ_0 and consequently decreasing ϵ would hence effectively increase the influence of such noise sources. The typical range for ϵ is 5 GHz to 10 GHz regarding the corresponding frequency. It cannot be much higher, as ϵ is limited because E_J cannot exceed the gap energy of the superconductor. In the case of transmons it is aluminium with a gap energy corresponding to about 80 GHz [21].

We set a reasonable limit for ϕ_0 such that $\tan^2(\frac{\phi_0}{2}) \approx \frac{1}{2}$, and set ϵ to about 10 GHz. Now let us get back to $|U| = \frac{1}{4}\tan^2(\frac{\phi_0}{2})\frac{\epsilon^2}{E_M}$, where $E_M = (\frac{\hbar}{e})^2\frac{1}{M}$ with the mutual inductance $M = k_M L$ between the qubits inductances L. We assume close coupling of the inductances by $k_M \approx 1$. Using these values one can estimate, that for $|U|$ to reach the threshold of 10 MHz discussed above, the energy of the transmons inductances $E_L = (\frac{\hbar}{e})^2\frac{1}{L}$ has to be at least about 100 MHz. Estimating a circular loop as inductance analogously to section 3.1.3, one finds that the radius r of such a loop would be $r \approx 60\,\mu\text{m}$. This is admittedly on the large side for transmons (their total size is of the

order of 100 µm), but definitely practicable. Also, figure 3.9 shows an example for a method to reduce the size of the loop drastically: Since the inductance depends strongly on the length of the wire piece, a zigzag structure can produce a large inductance on a relatively small scale. Note that the matching of the zigzag structure from the two coupled qubits also causes the coupling coefficient k_M to be close to one, as we assumed above. Also note that this causes a capacitance between the qubits to emerge, leading to an unwanted σ^x interaction. This exchange interaction of excitations between the qubits can however be suppressed by tuning the transmons to different energies $\epsilon_\uparrow$ and $\epsilon_\downarrow$, as an exchange of an interaction is then violating energy conservation. One can check that tuning the two chains in the emulator to different energies does not change the equivalence to the Fermi-Hubbard model, or any other result. The only aspect to account for is that the two chains then need separate coupling capacities, as the hopping term depends on the qubit energy (see equation (3.49)).

One should also mention that the inductance cannot be made too large, because E_L always has to stay large compared to E_J for the tunable transmon to function properly. The derivation in section 2.3 (and every other section performing circuit calculations with transmons involved) explicitly operated within this limit; otherwise the decoupling of the two intrinsic degrees of freedom would not work, as they are no longer energetically far apart. On the other hand we assumed moderate coherence times of $T_2^* = 1\,\mu s$ to get the threshold of 10 MHz for the parameter $|U|$. Better coherence times between 10 µs and 100 µs would give up to two additional orders of magnitude more room for the threshold.

In any case we showed how the realization of our emulator design is certainly an experimental challenge, yet possible with the current state of technology. More precise computer simulations for concrete circuit geometries have to follow now, to further analyze potential realizations of an emulator of the Fermi-Hubbard model.

For this theoretical thesis, the next question is how we want to initiate states in the emulator and how we intent to perform measurements.

Chapter 4

Initialization and Readout of the Emulator

As we have successfully derived a circuit for an emulator of the Fermi-Hubbard model in chapter 3, we will now address the questions how to initialize quantum states in it, as well as how we intend to obtain the emulation results by a readout procedure.

4.1 Initialization of a Transmon

Naturally, we start with the initialization of states in a transmon. Before we approach this process for the full emulator, we will explain it for a single transmon. It involves transmission line resonators coupled to a transmon. The transmission lines can be driven with microwave signals from the exterior.

This is a well-known procedure [11], but we will carefully derive how it functions, in order to obtain a proper understanding of it. We are then able to give analytic expressions of the crucial quantities concerning initialization, based on the quantities of the circuit and the microwave signals.

4.1.1 A Transmission Line

In superconducting circuits, a transmission line is realized by a long segment of superconducting metal with length l, which is also relatively broad. The circuit diagram is known from classical electrodynamics and shown in figure 4.1: The structure of a lossless transmission line contains a certain inductance per length L_0 and capacitance per length C_0 (towards ground); a resistance is neglected due to superconductivity, and we are anyhow not interested in dissipative effects regarding the transmission line. For the calculation we then assume it is made of n capacitors with capacitance $\frac{l}{n}C_0$ with a phase difference ϕ_j across these capacitors. They are then connected by n inductances with value $\frac{l}{n}L_0$, where we use continuous boundary conditions and introduce the phase $\phi_{n+1} = \phi_1$. This way, we can write down the Lagrangian using our familiar method

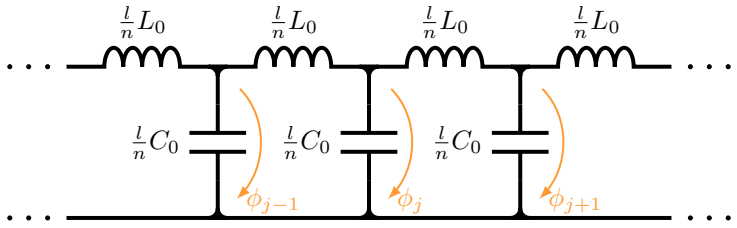

Figure 4.1: The circuit diagram of a transmission line of length l: With its given inductance per length L_0 and capacitance per length C_0 it is described by n capacitors with capacitance $\frac{l}{n}C_0$ connected through inductances $\frac{l}{n}L_0$. The phase difference across the j^{th} capacitor is denoted ϕ_j.

(using figure 2.2 from section 2.2.1) to be

$$\mathcal{L}_{\text{TL}} = \left(\frac{\hbar}{2e}\right)^2 \sum_{j=1}^{n} \left(\frac{1}{2}\frac{l}{n}C_0\dot{\phi}_j^2 - \frac{1}{2\frac{l}{n}L_0}(\phi_j - \phi_{j+1})^2\right), \tag{4.1}$$

which, with $N_j = \frac{1}{\hbar}\frac{\partial \mathcal{L}_{\text{TL}}}{\partial \dot{\phi}_j}$, trivially transforms to the Hamiltonian

$$H_{\text{TL}} = \frac{n}{l}\sum_{j=1}^{n}\left(\frac{1}{2}E_{C_0}N_j^2 + \frac{1}{2}E_{L_0}(\phi_j - \phi_{j+1})^2\right). \tag{4.2}$$

Here we have introduced the quantities $E_{C_0} = \frac{e^2}{C_0}$ and $E_{L_0} = (\frac{\hbar}{e})^2\frac{1}{L_0}$, which are therefore not energies, but have the dimensions energy times length.

To solve this problem of coupled harmonic oscillators, we define the set

$$K_n = \left\{\frac{2\pi}{l}j \mid j \in \{1,\dots,n\}\right\}, \tag{4.3}$$

and, for every $k \in K_n$, define the operators

$$P_k = \frac{1}{\sqrt{n}}\sum_{j=1}^{n} \mathrm{e}^{\mathrm{i}\frac{l}{n}kj}N_j, \text{ and } Q_k = \frac{1}{\sqrt{n}}\sum_{j=1}^{n}\mathrm{e}^{\mathrm{i}\frac{l}{n}kj}\phi_j. \tag{4.4}$$

This is of course a discrete Fourier transform and we know the inverse expressions

$$N_j = \frac{1}{\sqrt{n}}\sum_{k\in K_n}\mathrm{e}^{-\mathrm{i}\frac{l}{n}kj}P_j, \text{ and } \phi_j = \frac{1}{\sqrt{n}}\sum_{k\in K_n}\mathrm{e}^{-\mathrm{i}\frac{l}{n}kj}Q_k. \tag{4.5}$$

We utilize these expressions to study our Hamiltonian, where we first derive

$$\sum_{j=1}^{n}N_j^2 = \sum_{k,k'\in K_n}\underbrace{\sum_{j=1}^{n}\frac{1}{n}\mathrm{e}^{-\mathrm{i}\frac{l}{n}j(k+k')}}_{=\delta_{k,-k'}}P_kP_k' = \sum_{k\in K_n}P_kP_{-k} \tag{4.6}$$

and furthermore calculate

$$\begin{aligned}\sum_{j=1}^{n}(\phi_j-\phi_{j+1})^2 &= \sum_{k,k'\in K_n}\sum_{j=1}^{n}\frac{1}{n}\mathrm{e}^{-\mathrm{i}\frac{l}{n}jk}(1-\mathrm{e}^{-\mathrm{i}\frac{l}{n}k})Q_k\cdot\mathrm{e}^{-\mathrm{i}\frac{l}{n}jk'}(1-\mathrm{e}^{-\mathrm{i}\frac{l}{n}k'})Q'_k\\ &= \sum_{k,k'\in K_n}(1-\mathrm{e}^{-\mathrm{i}\frac{l}{n}k})(1-\mathrm{e}^{\mathrm{i}\frac{l}{n}k})Q_kQ_{-k}\\ &= \sum_{k,k'\in K_n}2(1-\cos(\frac{l}{n}k))Q_kQ_{-k}. \end{aligned} \tag{4.7}$$

This result leads us to the definition of

$$\Omega_k=\sqrt{E_{C_0}E_{L_0}}\sqrt{2(1-\cos(\frac{l}{n}k))}=2\sqrt{E_{C_0}E_{L_0}}\Big|\sin(\frac{l}{2n}k)\Big|, \tag{4.8}$$

where we used the addition theorem $1-\cos(\frac{l}{n}k)=2\sin^2(\frac{l}{2n}k)$. We also introduce $\mathfrak{m}=\frac{1}{E_{C_0}}$, which has not the dimension of mass, but is labelled like this for convenient notation, because we can now express our Hamiltonian as

$$H_{\mathrm{TL}}=\frac{n}{l}\sum_{k\in K_n}\left(\frac{1}{2\mathfrak{m}}P_kP_{-k}+\frac{\mathfrak{m}\Omega_k^2}{2}Q_kQ_{-k}\right). \tag{4.9}$$

In this form we recognize the structure of the harmonic oscillator and therefore define

$$a_k=\sqrt{\frac{\mathfrak{m}\Omega_k}{2}}(Q_k+\mathrm{i}\frac{1}{\mathfrak{m}\Omega_k}P_k). \tag{4.10}$$

Note that Q_k and P_k are not Hermitian, since $Q_k^\dagger=Q_{-k}$ and $P_k^\dagger=P_{-k}$, which can easily be seen in equation (4.4), if one regards that ϕ_j and N_j are Hermitian. By using $\Omega_{-k}=\Omega_k$, this leads to

$$Q_k=\sqrt{\frac{1}{2\mathfrak{m}\Omega_k}}(a_{-k}^\dagger+a_k),\ \text{and}\ P_k=\mathrm{i}\sqrt{\frac{\mathfrak{m}\Omega_k}{2}}(a_{-k}^\dagger-a_k). \tag{4.11}$$

However, we obtain our usual commutation relations because

$$[Q_k,P_{k'}]=\sum_{j,j'=1}^{n}\frac{1}{n}\mathrm{e}^{\mathrm{i}\frac{l}{n}(kj+k'j')}\underbrace{[\phi_j,N_j]}_{=\mathrm{i}\delta_{j,j'}}=\mathrm{i}\delta_{k,-k'} \tag{4.12}$$

and, regarding $\Omega_{-k}=\Omega_k$ and $[Q_k,Q_{k'}]=[P_k,P_{k'}]=0$, one can check that this gives

$$[a_k,a_{k'}^\dagger]=\delta_{k,k'}. \tag{4.13}$$

Using this relation after inserting the equations (4.11) in the Hamiltonian (4.9), one can

quickly check that the Hamiltonian can be written as

$$H_{\mathrm{TL}} = \frac{n}{l} \sum_{k \in K_n} \frac{1}{2} \Omega_k (a_{-k}^\dagger a_{-k} + a_k^\dagger a_k + 1) \tag{4.14}$$

and finally because $\Omega_{-k} = \Omega_k$ and $a_k = \frac{1}{\sqrt{n}} \sum_{j=1}^{n} \mathrm{e}^{\mathrm{i} \frac{l}{n} kj} \frac{\mathfrak{m}\Omega_k}{2} (\phi_j + \mathrm{i} \frac{1}{\mathfrak{m}\Omega_k} N_j)$, which results from combining the equations (4.10) and (4.4), we can see by symmetry that changing $-k \to k$ in the sum over $k \in K_n$ does not alter the result, therefore we get

$$H_{\mathrm{TL}} = \frac{n}{l} \sum_{k \in K_n} \Omega_k (a_k^\dagger a_k + \frac{1}{2}). \tag{4.15}$$

A transmission line is therefore a sum of harmonic oscillators with wavenumber k and energies $\frac{n}{l}\Omega_k$. These are the different modes that can be excited in the transmission line.

The value of the number n which tells us how many segments we need to assume for the transmission line is given by the fraction $\frac{l}{n}$, which is a characteristic length scale that stems from the microscopic properties of the material. The fraction is therefore very small. The transmission lines in superconducting circuits are very long compared to this length scale (their size is in the centimeter range), hence we can look at the continuum limit $n \to \infty$ and still get a valid description. Because of $\frac{n}{l} \sin(\frac{l}{2n} k) \to \frac{k}{2}$ for $n \to \infty$, we will now get a linear mode spectrum and performing this limit on our Hamiltonian leads to

$$H_{\mathrm{TL}} \to \sum_{k \in K_\infty} \hbar \omega_k (a_k^\dagger a_k + \frac{1}{2}), \tag{4.16}$$

where we introduced $K_\infty = \{\frac{2\pi}{l} j \mid j \in \mathbb{N}\}$ and $\hbar\omega_k = k\sqrt{E_{C_0} E_{L_0}}$. So we find, since we used continuous boundary conditions, an analogue to the classical case of standing waves in a circular structure: We find eigenmodes for any wavelength λ which is a fraction of the length of the structure (since $\frac{2\pi}{l} j = k = \frac{2\pi}{\lambda} \Rightarrow \lambda = \frac{l}{j}$, with $j \in \mathbb{N}$), where the eigenenergies of these modes increase linearly. The length of transmission lines is usually such, that the frequency of the energetically lowest mode is at the typical transmon energy of 5 GHz, which corresponds to a few centimeters.

4.1.2 A Transmon Coupled to a Transmission Line

We will now weakly couple a tunable transmon qubit to a transmission line by placing it into its proximity leading to a coupling through a capacitance C_g. The circuit diagram for this is given in figure 4.2. The transmon is denoted in the usual fashion with Josephson junctions J, shunt capacitances C, and loop inductance L, tuned by the external flux $\Phi_0 = \frac{\hbar}{2e}\phi_0$. Equal to section 4.1.1, the transmission line of length l is represented by n capacitances $\frac{l}{n} C_0$ linked through inductances $\frac{l}{n} L_0$, with the capacitance per length C_0 and the inductance per length L_0 of the transmission line. The capacitances C_g couple

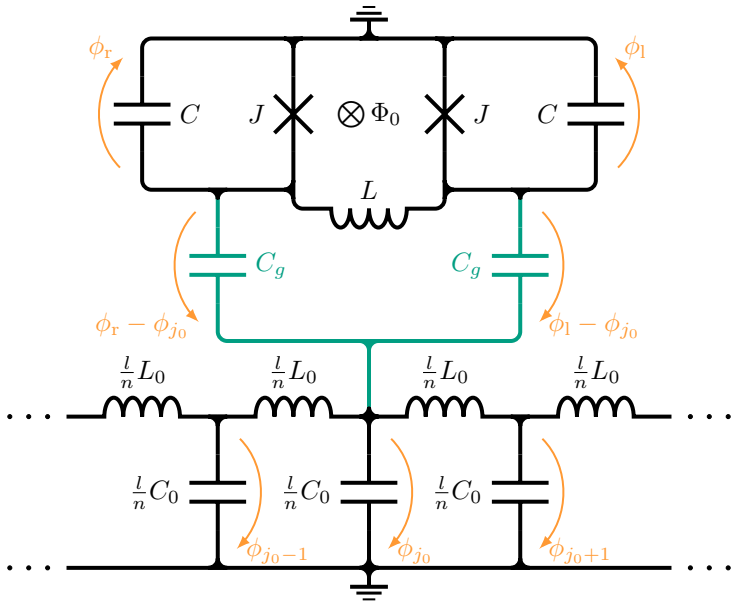

Figure 4.2: Circuit diagram of a transmon (as in figure 2.3 (b)) coupled to a transmission line (see figure 4.1) via coupling capacitances C_g, with parts of the qubit and the transmission line being grounded as a reference point. The phase differences across certain elements are denoted in orange. This setup leads to a coupling of the qubit via σ^x to the electrical field of the modes in the transmission line.

the transmon to the transmission line at the position of the j_0^{th} capacitor. One part of the transmon is grounded; we explained in section 3.1.1 that this is a valid description. The lower part of the transmission line is also grounded, as the capacitance per length of the transmission line on the chip is in fact the capacitance per length towards ground.

With the help of the circuit diagram in figure 4.2 and the denoted phases, using our usual method (see figure 2.2) we find the Lagrangian to be

$$\begin{aligned}\mathcal{L}_{\text{In}} = &\left(\frac{\hbar}{2e}\right)^2 \frac{1}{2} C(\dot{\phi}_l^2 + \dot{\phi}_r^2) + \frac{\hbar}{2e} I_c(\cos(\phi_l) + \cos(\phi_r)) - \left(\frac{\hbar}{2e}\right)^2 \frac{1}{2L}(\phi_l - \phi_r - \phi_0)^2 \\ &+ \left(\frac{\hbar}{2e}\right)^2 \sum_{j=1}^{n} \left(\frac{1}{2}\frac{l}{n} C_0 \dot{\phi}_j^2 - \frac{1}{2\frac{l}{n}L_0}(\phi_j - \phi_{j+1})^2\right) \\ &+ \left(\frac{\hbar}{2e}\right)^2 \frac{1}{2} C_g((\dot{\phi}_{j_0} - \dot{\phi}_l)^2 + (\dot{\phi}_{j_0} - \dot{\phi}_r)^2),\end{aligned} \tag{4.17}$$

where we used continuous boundary conditions via $\phi_{n+1} = \phi_1$, as in the previous section 4.1.1.

We continue as usual by introducing $\phi = \frac{1}{2}(\phi_l + \phi_r)$ and $\phi_- = \frac{1}{2}(\phi_l - \phi_r - \phi_0)$, and already fix the degree of freedom associated to ϕ_- to zero, hence $\phi_-, \dot{\phi}_- \approx 0$, with the justification for this explained in section 2.3. The external phase is also constant,

meaning $\dot{\phi}_0 = 0$. The Lagrangian can then be written as

$$\begin{aligned}\mathcal{L}_{\text{In}} &= \Big(\frac{\hbar}{2e}\Big)^2 C\dot{\phi}^2 + \frac{\hbar}{e} I_c \cos(\frac{\phi_0}{2})\cos(\phi) + \Big(\frac{\hbar}{2e}\Big)^2 \sum_{j=1}^{n} \left(\frac{1}{2}\frac{l}{n} C_0 \dot{\phi}_j^2 - \frac{1}{2\frac{l}{n}L_0}(\phi_j - \phi_{j+1})^2\right) \\ &\quad + \Big(\frac{\hbar}{2e}\Big)^2 C_g(\phi_{j_0} - \phi)^2 \\ &= \frac{1}{2}\Big(\frac{\hbar}{2e}\Big)^2 \boldsymbol{\phi}^{\mathrm{T}} A \boldsymbol{\phi} + \frac{\hbar}{e} I_c \cos(\frac{\phi_0}{2})\cos(\phi) \\ &\quad + \sum_{\substack{j=1 \\ j\neq j_0}}^{n} \Big(\frac{\hbar}{2e}\Big)^2 \frac{1}{2}\frac{l}{n} C_0 \dot{\phi}_j^2 - \sum_{j=1}^{n} \Big(\frac{\hbar}{2e}\Big)^2 \frac{1}{2\frac{l}{n}L_0}(\phi_j - \phi_{j+1})^2, \end{aligned} \tag{4.18}$$

where we introduced the vector $\boldsymbol{\phi} = (\phi, \phi_{j_0})$ and the matrix

$$A = \begin{pmatrix} 2(C + C_g) & 2C_g \\ 2C_g & \frac{l}{n}C_0 + 2C_g \end{pmatrix}. \tag{4.19}$$

The matrix is A is invertible with

$$A^{-1} = \frac{1}{2(C + C_g)(\frac{l}{n}C_0 + 2C_g) - 4C_g} \begin{pmatrix} \frac{l}{n}C_0 + 2C_g & 2C_g \\ 2C_g & 2(C + C_g) \end{pmatrix}, \tag{4.20}$$

so in the limit of weak coupling, and therefore $C_g \ll C, \frac{l}{n}C_0$, we find

$$A^{-1} \approx \begin{pmatrix} \frac{1}{2C} & \frac{n}{l}\frac{C_g}{CC_0} \\ \frac{n}{l}\frac{C_g}{CC_0} & \frac{n}{l}\frac{1}{C_0} \end{pmatrix}. \tag{4.21}$$

With the help of equation (4.21), we can easily transform the Lagrangian (4.18) to the Hamiltonian

$$\begin{aligned} H_{\text{In}} &= E_C N^2 - E_J \cos(\frac{\phi_0}{2})\cos(\phi) + \frac{n}{l}\sum_{j=1}^{n}\left(\frac{1}{2}E_{C_0}N_j^2 + \frac{1}{2}E_{L_0}(\phi_j - \phi_{j+1})^2\right) \\ &\quad + \frac{1}{4}\frac{C_g}{\frac{l}{n}C_0} E_C N N_{j_0}, \end{aligned} \tag{4.22}$$

with $N_{(j)} = \frac{1}{\hbar}\frac{\partial \mathcal{L}_{\text{In}}}{\partial \dot{\phi}_{(j)}}$, as well as $E_{C_{(0)}} = \frac{e^2}{C_{(0)}}$, $E_J = \frac{\hbar}{e} I_{\text{c}}$ and $E_{L_0} = (\frac{\hbar}{e})^2 \frac{1}{L_0}$. Using our findings of the sections 2.3 and 4.1.1, especially equations (2.15), (2.18) and (4.15) and the insertion of equation (4.11) in (4.5) (keep in mind that in the sum over K_n one can replace $-k \to k$), we can rewrite this as

$$\begin{aligned} H_{\text{In}} &= \frac{1}{2}\epsilon\sigma^z + \frac{n}{l}\sum_{k\in K_n} \Omega_k (a_k^\dagger a_k + \frac{1}{2}) \\ &\quad + \mathrm{i}\frac{1}{8}\frac{C_g}{lC_0}\Big(\frac{E_{L_0}}{E_{C_0}}\Big)^{\frac{1}{4}} \sqrt{E_C}\epsilon\sigma^x \sum_{k\in K_n} \sqrt{n\sin(\frac{l}{2n}k)}(\mathrm{e}^{\mathrm{i}\frac{l}{n}kj_0}a_k^\dagger - \mathrm{e}^{-\mathrm{i}\frac{l}{n}kj_0}a_k). \end{aligned} \tag{4.23}$$

As a last step we perform the continuum limit $n \to \infty$, as in the previous section 4.1.1.

In this limit we find $n\sin(\frac{l}{2n}k) \to \frac{1}{2}lk$. A bit more subtle is the treatment of the phase factor $\mathrm{e}^{\pm\mathrm{i}\frac{l}{n}kj_0}$: The position x_0 between zero and l, where the qubit is placed next to the transmission line is fixed, the number j_0 of the capacitor the transmon couples to adjusts depending on n, such that the fraction $\frac{l}{n}j_0$ is fixed with regard to n and we have to replace $\mathrm{e}^{\pm\mathrm{i}\frac{l}{n}kj_0} \to \mathrm{e}^{\pm\mathrm{i}kx_0}$. If we also use equation (4.16), we see that in the limit $n \to \infty$ we find

$$H_{\mathrm{In}} \to \frac{1}{2}\epsilon\sigma^z + \sum_{k\in K_\infty} \hbar\omega_k a_k^\dagger a_k + \mathrm{i}g_{\mathrm{In}}\sigma^x \sum_{k\in K_\infty} lk(\mathrm{e}^{\mathrm{i}kx_0}a_k^\dagger - \mathrm{e}^{-\mathrm{i}kx_0}a_k), \tag{4.24}$$

with the coupling energy

$$g_{\mathrm{In}} = \frac{1}{16}\frac{C_g}{C_{\mathrm{TL}}}\Big(\frac{E_{L_{\mathrm{TL}}}}{E_{C_{\mathrm{TL}}}}\Big)^{\frac{1}{4}}\sqrt{E_C\epsilon}, \tag{4.25}$$

where we introduced the total capacitance $C_{\mathrm{TL}} = lC_0$ and total inductance $L_{\mathrm{TL}} = lL_0$ of the transmission line, and the usual corresponding energies $E_{C_{\mathrm{TL}}} = \frac{e^2}{C_{\mathrm{TL}}}$ as well as $E_{L_{\mathrm{TL}}} = (\frac{\hbar}{e})^2\frac{1}{L_{\mathrm{TL}}}$. The phase factor in the sum can classically be interpreted as the phase of the electric field of a standing wave with wavenumber k in the transmission line depending on the position x_0, which varies of course with the position. Note that the factor lk in the sum of the coupling term causes the coupling energy of each mode to be constant relative to the frequency ω_k, which also increases linearly in k (see the definition following equation (4.16)).

As a remark: One aspect one should be careful about in the continuum limit is that one would not couple to a single capacitor in the transmission line anymore. Instead, one would need to introduce also a coupling capacity per length in the circuit diagram in figure 4.2 and couple to multiple capacitors in the transmission line next to the transmon. In this more detailed analysis one would end up with an interaction with an average over the phase factor $\mathrm{e}^{\pm\mathrm{i}kx}$ with x going from one end of the transmon to the other. We are however only interested in the excitations of the transmission line with wavelengths in the centimeter range, as they correspond to the qubit energy scale. This is however very large compared to the qubit size, therefore the phase factor would only change little and the above description is sufficient.

One should also mention that inductive coupling leading to an additional σ^z interaction of the transmon with the transmission line can be neglected here, as it is much weaker than the capacitive coupling.

With the necessary tools in hand, we can now continue with the initialization process.

4.1.3 Initialization through Rabi Oscillation

By now, we have established how a transmission line works and how we can couple it to a qubit. This section continues by explaining how this setup can be used to initiate a qubit from its ground state $|0\rangle$ to its excited state $|1\rangle$. We will do this through the process of Rabi oscillation. To understand this procedure, we start by deriving the relevant

Hamiltonian: Our qubit with energy splitting ϵ is coupled via σ^x to the modes of a transmission line with coupling energy g_R. We select one distinct mode with frequency ω, and denote the creation and annihilation operators of this mode $a^\dagger$ and a. The Hamiltonian can be written as

$$H_\mathrm{R} = \frac{1}{2}\epsilon\sigma^z + \hbar\omega a^\dagger a + g_\mathrm{R}\sigma^x(a^\dagger + a), \tag{4.26}$$

where we simplified the coupling term a bit notation wise; one can check that this is still equivalent to equation (4.24).

To start further studying, we will treat the resonator part separately in a semiclassical approach. Assume just the simple Hamiltonian $H = \hbar\omega a^\dagger a$ of a resonator. Switching to the Heisenberg picture, one finds the time dependent operators $a^\dagger \mapsto a^\dagger \mathrm{e}^{\mathrm{i}\omega t}$ and $a \mapsto a\mathrm{e}^{-\mathrm{i}\omega t}$. Also assume that we externally drive this mode of the transmission line. This situation of classical driving can be described by the creation of a coherent state $|\alpha\rangle$ (with $\alpha \in \mathbb{C}$) in the resonator, where $|\alpha\rangle = D(\alpha)|0\rangle$ with the vacuum ground state $|0\rangle$ and the displacement operator $D(\alpha) = \mathrm{e}^{\alpha a^\dagger - \alpha^* a}$. We introduced that operator in section 3.2.2 following equation (3.39). With the relations for the displacement operator mentioned in that section, we can easily see that $\langle\alpha|a^\dagger|\alpha\rangle = \alpha^*$ and $\langle\alpha|a|\alpha\rangle = \alpha$. Finally, writing $\alpha = |\alpha|\mathrm{e}^{\mathrm{i}\varphi}$ with $\varphi \in \mathbb{R}$, we can semiclassically replace $a^\dagger + a \mapsto \langle\alpha|(a^\dagger \mathrm{e}^{\mathrm{i}\omega t} + a\mathrm{e}^{-\mathrm{i}\omega t})|\alpha\rangle = 2|\alpha|\cos(\omega t - \varphi)$ in the Hamiltonian H_R giving

$$H_\mathrm{R} = \frac{1}{2}\epsilon\sigma^z + 2g_\mathrm{R} f\cos(\omega t)\sigma^x, \tag{4.27}$$

where we ignored the qualitatively irrelevant phase φ and introduced $f = |\alpha|$ for a more convenient notation. We also dropped the resonator energy, since $\langle\alpha|a^\dagger a|\alpha\rangle = |\alpha|^2 = f^2$ is a constant now. Note too, that f^2 gives the mean number of photons in the resonator, which means that f is proportional to the amplitude of the electrical field in the resonator and therefore a measure for the strength of our driving.

We continue by transforming the Hamiltonian into a rotating frame with the unitary transformation $U = \mathrm{e}^{-\mathrm{i}\frac{1}{2}\omega\sigma^z t}$. Because this transformation is time dependent, the time evolution in this frame is given by the Hamiltonian

$$\tilde{H}_\mathrm{R} = \mathrm{i}\hbar\dot{U}^\dagger U + U^\dagger H U. \tag{4.28}$$

Since $[\sigma^z, \sigma^\pm] = \pm 2\sigma^\pm$, one can derive $U^\dagger\sigma^\pm U = \sigma^\pm e^{\pm\mathrm{i}\omega t}$, using Baker-Campbell-Hausdorff identities. With $\sigma^x = \sigma^+ + \sigma^-$ and after applying a rotating wave approximation, where fast oscillating terms $\mathrm{e}^{\pm\mathrm{i}2\omega t}$ are averaged out to zero (the frequency is in the gigahertz range), one finds that

$$\tilde{H}_\mathrm{R} = \frac{1}{2}(\epsilon - \hbar\omega)\sigma^z + g_\mathrm{R} f\sigma^x. \tag{4.29}$$

We now look at the time evolution of a state $|\psi(t)\rangle$ that is in the ground state of the qubit in the beginning, hence $|\psi(0)\rangle = |0\rangle$. For this we assume our system to be

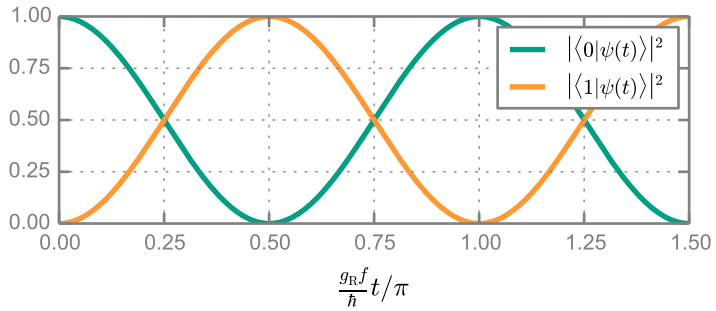

Figure 4.3: Rabi oscillation of a qubit state $|\psi(t)\rangle$, starting in the ground state $|0\rangle$. The qubit is coupled via σ^x to the electric field in a transmission line, with coupling strength g_R. The electric field is driven with a frequency ω and f is a dimensionless measure for the amplitude of the field, as f^2 is the mean number of photons in the resonator. The qubit energy ϵ is such that it fulfills the resonance condition $\epsilon = \hbar\omega$. This causes the pictured Rabi oscillation between ground state $|0\rangle$ and excited state $|1\rangle$. Applying a microwave pulse of the right length and strength and frequency can therefore flip a qubit in its excited state.

tuned such that the qubit energy is in resonance with the mode in the transmission line, which means $\epsilon = \hbar\omega$. This simplifies the Hamiltonian to $\tilde{H}_\mathrm{R} = g_\mathrm{R} f \sigma^x$, and if we use the representation $\mathrm{e}^{-\mathrm{i}\frac{g_\mathrm{R} f}{\hbar}\sigma^x t} = \cos(\frac{g_\mathrm{R} f}{\hbar}t)\mathbb{1} - \mathrm{i}\sin(\frac{g_\mathrm{R} f}{\hbar}t)\sigma^x$ (which can be easily derived by using the exponential series and $(\sigma^x)^2 = \mathbb{1}$), the time evolution becomes

$$|\psi(t)\rangle = \mathrm{e}^{-\frac{\mathrm{i}}{\hbar}\tilde{H}_\mathrm{R} t} = \cos(\frac{g_\mathrm{R} f}{\hbar}t)|0\rangle - \mathrm{i}\sin(\frac{g_\mathrm{R} f}{\hbar}t)|1\rangle \text{ for } \epsilon = \hbar\omega. \tag{4.30}$$

This means the qubit performs a Rabi oscillation between its ground state $|0\rangle$ and its excited state $|1\rangle$ as illustrated in figure 4.3. We can immediately see now, how we can initiate a qubit in the state $|1\rangle$: The system is in its ground state in the beginning (which it will be eventually if one just waits long enough). Tuning the qubit in resonance with the mode it is coupled to, and applying a driving field for a time t such that $\frac{g_\mathrm{R} f}{\hbar}t = \frac{\pi}{2}$ (or any other odd multiple of $\frac{\pi}{2}$) will flip the qubit into the excited state $|1\rangle$. After turning off the field, the qubit stays in that state, at least until decoherence or dephasing will destroy the state. This is how it is typically done in experiments, where the qubit is on resonance with a mode in a coupled transmission line and a distinct microwave pulse is applied in the transmission line, such that the qubit is flipped.

Alternatively one could leave the microwave driving on constantly and tune and detune the resonance between qubit and mode. This is possible since the detuning is also suppressing the transition from ground to excited state because the transition is in this case not energy conserving, which can be seen in the Hamiltonian in equation (4.29) for $\epsilon - \hbar\omega \neq 0$. This is however not how it is done in practice, as the microwave pulses are much easier to control.

Now that the initiation process is understood, we can advance to the readout measurement of transmons.

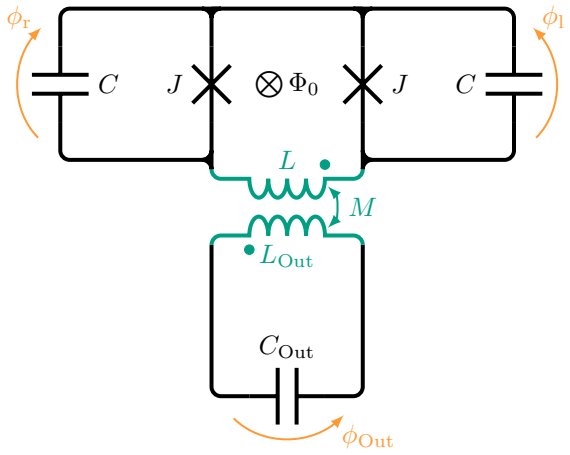

Figure 4.4: Circuit diagram of a transmon (as in figure 2.3 (b)) coupled to an LC circuit that represents a resonator, with inductance L_Out and capacitance C_Out. The inductance L of the transmon and the inductance L_Out of the resonator form a mutual inductance $M = k_M\sqrt{LL_\mathrm{Out}}$ with $k_M \in (0,1)$. The mutual inductance causes a coupling of the operator σ^z of the qubit to the electrical field of the resonator.

4.2 Readout of a Transmon

We would like to obtain information about the excitations in the fermionic system we emulate. This corresponds to measurements of the σ^z operators of the emulator (remember equation (2.26)). To perform this task, we suggest an analogous coupling mechanism to section 3.2.2, since we saw in this section, that coupling to the inductance of a transmon results in coupling to its σ^z operator. We suggest to couple a readout resonator to the transmon by a mutual inductance as pictured in figure 4.4: Instead of modeling the resonator by a transmission line like we did for the initialization process in section 4.1, we use only one distinct mode and model the resonator by an LC circuit. The eigenfrequency of this LC circuit should be large compared to the qubit energy, because in this case we can neglect capacitive coupling between resonator and qubit that would result in a σ^x-type coupling (see section 4.1.2), because such a term contributes an exchange interaction of excitations which would then not be energy conserving. This is a valid representation for a small resonator, with the lowest mode being energetically high due to a small wavelength (see the mode spectrum of a transmission line in section 4.1.1).

Let us study the circuit in figure 4.4: We have the usual transmon with Josephson junctions J and shunt capacities C, and loop inductance L. The phase differences across the junctions are denoted ϕ_l and ϕ_r, the transmon is tuned through an external flux $\Phi_0 = \frac{\hbar}{2e}\phi_0$. The LC circuit consists of an inductance L_Out and a capacitance C_Out, with a phase difference ϕ_Out across these elements. An external magnetic flux through the LC circuit is ignored. The two inductances in the circuit form a mutual inductance $M = k_M\sqrt{LL_\mathrm{Out}}$ with $k_M \in (0,1)$. We can derive the Lagrangian of this system using

figure 2.2 and the treatment of a mutual inductance in equation (3.32):

$$\begin{aligned}\mathcal{L}_{\mathrm{Out}} = &\Big(\frac{\hbar}{2e}\Big)^2\frac{1}{2}C(\dot{\phi}_{\mathrm{l}}^2+\dot{\phi}_{\mathrm{r}}^2)+\Big(\frac{\hbar}{2e}\Big)^2\frac{1}{2}C_{\mathrm{Out}}\dot{\phi}_{\mathrm{Out}}^2+\frac{\hbar}{2e}I_{\mathrm{c}}(\cos(\phi_{\mathrm{l}})+\cos(\phi_{\mathrm{r}}))\\ &-\Big(\frac{\hbar}{2e}\Big)^2\frac{1}{1-k_M^2}\Big(\frac{1}{2L}(\phi_{\mathrm{l}}-\phi_{\mathrm{r}}-\phi_0)^2+\frac{1}{2L_{\mathrm{Out}}}\phi_{\mathrm{Out}}^2\Big)\\ &+\Big(\frac{\hbar}{2e}\Big)^2\frac{k_M}{1-k_M^2}\frac{1}{\sqrt{LL_{\mathrm{Out}}}}(\phi_{\mathrm{l}}-\phi_{\mathrm{r}}-\phi_0)\phi_{\mathrm{Out}}.\end{aligned} \tag{4.31}$$

We continue with the transformation of variables already used in section 2.3, and introduce $\phi=\frac{1}{2}(\phi_{\mathrm{l}}+\phi_{\mathrm{r}})$ as well as $\phi_-=\frac{1}{2}(\phi_{\mathrm{l}}-\phi_{\mathrm{r}}-\phi_0)$, which—using $\dot{\phi}_0=0$ and the addition theorems for the cosine—gives

$$\begin{aligned}\mathcal{L}_{\mathrm{Out}} = &\Big(\frac{\hbar}{2e}\Big)^2C(\dot{\phi}^2+\dot{\phi}_-^2)+\Big(\frac{\hbar}{2e}\Big)^2\frac{1}{2}C_{\mathrm{Out}}\dot{\phi}_{\mathrm{Out}}^2+\frac{\hbar}{e}I_{\mathrm{c}}\cos(\phi_-+\frac{\phi_0}{2})+\cos(\phi)\\ &-\Big(\frac{\hbar}{2e}\Big)^2\frac{1}{1-k_M^2}\Big(\frac{1}{2L}\phi_-^2+\frac{1}{2L_{\mathrm{Out}}}\phi_{\mathrm{Out}}^2\Big)+\Big(\frac{\hbar}{2e}\Big)^2\frac{k_M}{1-k_M^2}\frac{1}{\sqrt{LL_{\mathrm{Out}}}}\phi_-\phi_{\mathrm{Out}},\end{aligned} \tag{4.32}$$

and we can now transform to the Hamiltonian

$$\begin{aligned}H_{\mathrm{Out}} = &E_C(N^2+N_-^2)+\frac{1}{2}E_{C_{\mathrm{Out}}}N_{\mathrm{Out}}^2-E_J\cos(\phi_-+\frac{\phi_0}{2})\cos(\phi)\\ &+\frac{1}{2}E_L\xi\phi_-^2+\frac{1}{8}E_{L_{\mathrm{Out}}}\phi_{\mathrm{Out}}^2+\tilde{g}\phi_-\phi_{\mathrm{Out}},\end{aligned} \tag{4.33}$$

with the usual canonical momentums $N_{(\cdot)}=\frac{1}{\hbar}\frac{\partial\mathcal{L}_{\mathrm{Out}}}{\partial\dot{\phi}_{(\cdot)}}$ and energies $E_{C_{(\mathrm{Out})}}=\frac{e^2}{C_{(\mathrm{Out})}}$, $E_J=\frac{\hbar}{e}I_{\mathrm{c}}$ as well as $E_{L_{(\mathrm{Out})}}=(\frac{\hbar}{e})^2\frac{1}{L_{(\mathrm{Out})}}$. We also introduced $\xi=\frac{1}{1-k_M^2}$ and the coupling energy $\tilde{g}=-\frac{1}{2}(\frac{\hbar}{e})^2\frac{1}{\sqrt{LL_{\mathrm{Out}}}}k_M\xi$.

Following the same argument as in section 3.2.2, we consider that—in a transmon—E_L is large compared to E_J, which justifies expanding $E_J\cos(\phi_-+\frac{\phi_0}{2})$ for small ϕ_-, since terms of the form $E_J\phi_-^2$ are negligible towards terms of the form $E_L\phi_-^2$. This leads us to

$$\begin{aligned}H_{\mathrm{Out}} = &E_C(N^2+N_-^2)+\frac{1}{2}E_{C_{\mathrm{Out}}}N_{\mathrm{Out}}^2-E_J\cos(\frac{\phi_0}{2})\cos(\phi)+E_J\sin(\frac{\phi_0}{2})\cos(\phi)\phi_-\\ &+\frac{1}{2}E_L\xi\phi_-^2+\frac{1}{8}E_{L_{\mathrm{Out}}}\phi_{\mathrm{Out}}^2+\tilde{g}\phi_-\phi_{\mathrm{Out}}.\end{aligned} \tag{4.34}$$

We identify the usual qubit energy terms $E_CN^2-E_J\cos(\frac{\phi_0}{2})\cos(\phi)=\frac{1}{2}\epsilon\sigma^z$ from equation (2.15), harmonic oscillators $E_CN_-^2+\frac{1}{2}E_L\xi\phi_-^2=\hbar\omega_-a_-^\dagger a_-$ and $\frac{1}{2}E_{C_{\mathrm{Out}}}N_{\mathrm{Out}}^2+\frac{1}{8}E_{L_{\mathrm{Out}}}\xi\phi_{\mathrm{Out}}^2=\hbar\omega a^\dagger a$, with $\hbar\omega_-=\sqrt{2E_CE_L\xi}$ and $\hbar\omega=\frac{1}{2}\sqrt{E_{C_{\mathrm{Out}}}E_{L_{\mathrm{Out}}}\xi}$. We therefore obtain $\phi_-=\frac{1}{\sqrt{2}}(\frac{2E_C}{\xi E_L})^{\frac{1}{4}}(a_-^\dagger+a_-)$ as well as $\phi_{\mathrm{Out}}=\frac{1}{\sqrt{2}}(\frac{4E_{C_{\mathrm{Out}}}}{\xi E_{L_{\mathrm{Out}}}})^{\frac{1}{4}}(a^\dagger+a)$. We also use equation (2.19) to write $\cos(\phi)=\alpha^z\sigma^z+\beta\mathbb{1}$ with $\alpha^z=-\frac{1}{4}(\frac{2E_C}{E_J\cos(\phi_0/2)})^{\frac{1}{2}}$. Neglecting constant contributions, the Hamiltonian can now be rewritten as

$$H_{\mathrm{Out}}=\frac{1}{2}\epsilon\sigma^z+\hbar\omega a^\dagger a+\hbar\omega_-a_-^\dagger a_-+g_-\sigma^z(a_-^\dagger+a_-)+g(a^\dagger+a)(a_-^\dagger+a_-), \tag{4.35}$$

with $g_- = \frac{1}{\sqrt{2}} \sin(\frac{\phi_0}{2}) \alpha^z (\frac{2E_C}{\xi E_L})^{\frac{1}{4}} E_J$ and $g = -\frac{1}{4} k_M \xi (\frac{8 E_C E_{C_{\text{Out}}}}{\xi^2 E_L E_{L_{\text{Out}}}})^{\frac{1}{4}} (\frac{\hbar}{e})^2 \frac{1}{\sqrt{E_L E_{L_{\text{Out}}}}}$.

We are now in a similar situation to equation (3.39) in section 3.2.2. We therefore proceed similarly and use the displacement operator $D(d) = \mathrm{e}^{d a_-^\dagger - d^\dagger a_-}$ to define the unitary transformation

$$U = D(-\frac{1}{\hbar \omega_-} g_- \sigma^z), \tag{4.36}$$

and by applying the identities for the displacement operator following equation (3.39), we find

$$U^\dagger H_{\text{Out}} U = \frac{1}{2} \epsilon \sigma^z + \hbar \omega a^\dagger a + \hbar \omega_- a_-^\dagger a_- + g(a^\dagger + a)(a_-^\dagger + a_-) + g_{\text{Out}} \sigma^z (a^\dagger + a), \tag{4.37}$$

with $g_{\text{Out}} = -\frac{2 g g_-}{\hbar \omega_-}$. We again neglect the high energy degree of freedom of the transmon by fixing $a_-^\dagger a_-, a_-^\dagger + a_- \approx 0$ and arrive at the effective Hamiltonian

$$H_{\text{Out,eff}} = \frac{1}{2} \epsilon \sigma^z + \hbar \omega a^\dagger a + g_{\text{Out}} \sigma^z (a^\dagger + a), \tag{4.38}$$

with the coupling energy

$$g_{\text{Out}} = -\frac{2 g g_-}{\hbar \omega_-} = -\frac{1}{8} k_M (1 - k_M^2)^{\frac{1}{4}} \tan(\frac{\phi_0}{2}) \frac{\epsilon}{E_L} \Big(\frac{E_{C_{\text{Out}}}}{E_{L_{\text{Out}}}} \Big)^{\frac{1}{4}} \Big(\frac{\hbar}{e} \Big)^2 \frac{1}{\sqrt{L L_{\text{Out}}}}. \tag{4.39}$$

We found an effective interaction between the σ^z operator of the qubit and the electric field $a^\dagger + a$ in the resonator. This gives the possibility to measure the state in which the qubit is in and subsequently the corresponding fermionic excitations in the Fermi-Hubbard model.

Alternatively, one could use the standard approach for qubit readout [11]. It would involve coupling the qubit capacitively to a readout resonator. For a large detuning of the resonator frequency and the qubit energy one obtains an effective shift of the resonator frequency depending on the qubit state, which allows for projective measurements of the qubit state trough spectroscopy. This will however not be presented here in detail.

Since we have established how we can readout the state of an individual qubit with the help of readout resonators, and discussed the initialization of individual qubits in the preceding section 4.1, we can continue by discussing a full initialization and readout scheme for the emulator consisting of multiple coupled qubits.

4.3 Treating Multiple Transmons

One aspect to consider in the emulator in contrast to the initialization and readout procedures for individual qubits, is that the qubits in the emulator are coupled to each other by their σ^z and σ^x operators. First of all, we state that in fact—for small coupling energies—the readout is not influenced by this.

We investigate the initialization process in more detail. For this we use the Hamiltonian (4.26) of a qubit coupled to the electrical field of a resonator, and add a second qubit which is coupled to the first one. Let us start with an additional σ^z interaction. This gives a Hamiltonian of the form

$$H_{\mathrm{R}}^z = \frac{1}{2}\epsilon\sigma_1^z + \frac{1}{2}\epsilon\sigma_2^z + \hbar\omega a^\dagger a + g^z\sigma_1^z\sigma_2^z + g_{\mathrm{R}}\sigma_1^x(a^\dagger + a). \tag{4.40}$$

During the initialization, we can consider the second qubit to either still be in the ground state, or already be flipped up and in its excited state. This allows to use $\langle\sigma_2^z\rangle = \pm 1$ and we can effectively write

$$H_{\mathrm{R}}^z = \frac{1}{2}(\epsilon \pm 2g^z)\sigma_1^z + \hbar\omega a^\dagger a + g_{\mathrm{R}}\sigma_1^x(a^\dagger + a). \tag{4.41}$$

The initialization process for qubit number one is therefore identical, except for the resonance condition $\hbar\omega = \epsilon$ from section 4.1.3 being shifted to $\hbar\omega = \epsilon \pm 2g^z$.

The situation of the two qubits being coupled by σ^x is more difficult. The Hamiltonian of this setup reads

$$H_{\mathrm{R}}^x = \frac{1}{2}\epsilon\sigma_1^z + \frac{1}{2}\epsilon\sigma_2^z + \hbar\omega a^\dagger a + g^x\sigma_1^x\sigma_2^x + g_{\mathrm{R}}\sigma_1^x(a^\dagger + a). \tag{4.42}$$

Since the initialization takes time (see figure 4.3), while exciting one qubit, it starts exciting the neighboring qubit as well by exchanging its excitation through the σ^x-type coupling. This leads to an oscillation that interferes with the Rabi oscillation of exciting qubit one through the resonator. If we would like to excite qubit number one and keep qubit number two in its ground state, we have to find a time to match these interfering oscillations accordingly. This potentially takes much longer than the excitation of a single qubit. Moreover, it becomes especially difficult, when we consider a chain of many coupled qubits. One could operate in the limit of strong driving, thus lowering the time scale of the initialization through the electric field such that it is much faster than the exchange of energy between the qubits. While this would work in theory, it has distinct disadvantages such as increasing the temperature in the system and—more importantly—it increases the likelihood of exciting a qubit in excited states above the first excited state; this can be derived from the upcoming discussion in section 5.2, where we will treat such problematic excitations.

We suggest an easy solution to this problem: If we pairwise detune the qubits from resonance to different energies, their σ^x interaction is effectively suppressed, since the resulting transitions are in this case not energy conserving. This gives individual control over the qubits, and an arbitrary combination of excitations can be initialized in the emulator. The emulation would also be frozen during the initialization process and would not start until the qubits are brought back to degeneracy.

Figure 4.5 presents a possible scheme for initialization and readout: Two transmission lines are coupled to the left part of the emulator. For example an applicable field

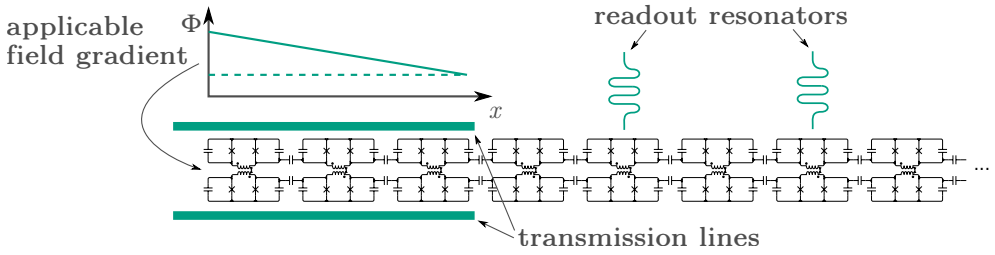

Figure 4.5: Initialization and readout scheme for our emulator of the Fermi-Hubbard model from figure 3.6. A part on the left of the emulator is coupled to transmission lines for initialization, where an applicable field gradient in that part is used to pairwise detune the qubits, such that the σ^x coupling between neighboring qubits is suppressed. They can then be excited individually to initialize a certain quantum state in the emulator. Turning off the field gradient brings the transmons back to degeneracy and starts the emulation, since the coupling is then restored. Readout resonators coupled to single qubits at distinct locations are used to obtain information about the quantum state in the emulator after the system has evolved.

gradient could detune the transmons. The qubits in this part of the emulator could then be initialized individually. Deactivating the field gradient would then start the emulation. Readout resonators coupled to qubits at distinct locations could deliver information about the emulation after the system has evolved over a certain time.

Chapter 5

Discussion of Errors

We have established the full circuit of an emulator for the Fermi-Hubbard model as well as how we intend to initialize a quantum state in it and read out emulation results afterwards. Naturally, the next step is a discussion of errors in the emulator and its results of emulation. We do not have quantum error correction available in the emulator, so this is not merely an obligatory task. In our context of quantum emulation, an error discussion is closely linked to the four criteria from section 2.1, which a quantum emulator should satisfy. Particularly the third criterion of reliability is directly connected to errors in the emulator: The results an emulator produces should correspond faithfully to a quantity of the ideal model one seeks to emulate. This is obviously not the case if the emulation contains large errors. Moreover, this is especially difficult to quantify, since an emulator should produce results, which are otherwise not available through analytic calculation or numerical simulation; so they cannot be trivially compared to any reference value.

This chapter addresses this problem by briefly investigating certain error sources. We discuss possible solutions to deal with the difficulty of quantifying the errors on the emulation results.

5.1 Temperature and Disorder of the Emulator

In this section we address two sources of error in a quantum emulator, that are present in any design for an emulator.

Let us start with the impact of temperature on the system. The transmons are operated at a temperature of $T = 20\,\mathrm{mK}$, which corresponds to a frequency of 400 MHz. The qubit energy ϵ on the other hand is above 5 GHz, hence an order of magnitude larger. This leads us to our postulate that effects related to temperature are suppressed through the very small prefactor $\mathrm{e}^{-\frac{\epsilon}{k_\mathrm{B}T}} \approx \mathrm{e}^{-10}$ from the Boltzmann distribution (with the Boltzmann constant k_B of course). For example, 400 MHz is larger than typical coupling energies of superconducting qubits to resonators for initialization or readout, yet these processes are working fine in experiments. Moreover, the energy scale correspond-

ing to coherence times higher than 1 µs are lower than 1 MHz. We see this as evidence supporting our postulate that our emulator using superconducting devices effectively operates at zero temperature. This would be an example of a great advantage towards similar emulators using cold gases, where the temperature of the system, which can in reality never be brought down to zero, ends up to be an effective temperature of the emulated system as well. Naturally, more rigorous study of this issue needs to follow to reinforce our claim.

Another obvious source of error is disorder in the system, which means certain derivations in the quantities of the Hamiltonian. We focus on the strongest source of disorder in our superconducting circuit: Because our circuits are macroscopic in size, purely geometric quantities like capacitances or inductances are fairly exact to manufacture. The precision of the printing process of chips is far more accurate than the size of the printed structures. This does not apply to the manufacturing of the Josephson junctions, since their behavior is determined by the constitution of the weak link between the two sides of the junction. In aluminium junctions, this link is constructed by printing one lead, letting it build up a thin layer of oxide and then print the second lead on top. The precise structure of the oxide layer is however very hard to control, and on its microscopic scale, tiny variations in the oxidation process have relatively large effects on the properties of the junction [9].

We therefore focus on disorder in the energy E_J associated with the Josephson junctions. We do this by introducing derivations from the mean value by $E_J \to E_J + \delta E_J$. The parameters U and t of the Fermi-Hubbard model (2.27) we intend to emulate show, according to equations (3.48) and (3.49), the proportionalities $U \propto \epsilon^2$ and $t \propto \epsilon$. Since it holds that $\epsilon \propto \sqrt{E_J}$ for the transmon energies (see equation (2.16)), we can quantify the effect of disorder in E_J via $U \to U + \delta U$, $t \to t + \delta t$, by

$$\delta U = \frac{\delta E_J}{E_J} U, \text{ and } \delta t = \frac{1}{2} \frac{\delta E_J}{E_J} t. \tag{5.1}$$

We now know to which extent the parameters in our emulator vary. This gives rise to a very difficult question: How can we quantify to which extent this affects the results of emulation compared to an ideal system? We intend to emulate problems that are not accessible through other approaches like analytic calculations or numeric simulations on a classical computer. If we do not know a solution to the ideal system, it is apparent that a calculation of deviations towards a non-ideal system is a highly nontrivial task. Theoretical groundwork to address this issue needs to be established; especially since this affects quantum emulation without error correction in general.

5.2 The Third Energy Level of a Transmon

A specific possible source of error in our emulator design is that a transmon is not a strict two level system: Section 2.3 explained that in fact the transmon is an anharmonic oscillator. Obviously, excitations of the second excited state would have no correspon-

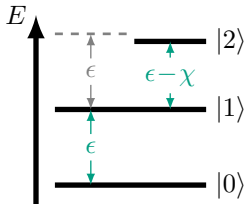

Figure 5.1: Energy spectrum of the first three levels of a transmon. The energy difference between the ground state $|0\rangle$ and the first excited state $|1\rangle$ is ϵ. Since the transmon is an anharmonic oscillator, above these levels is a third level $|2\rangle$, with an energy difference $\epsilon - \chi$ towards the state $|1\rangle$, with the anharmonicity χ. Common values for χ are approximately $\frac{\epsilon}{10}$.

dence in the fermionic system we wish to emulate. Therefore we have to check, if such excitations are sufficiently unlikely.

To investigate this problem, instead of projecting the operators $a^\dagger a$ and $a^\dagger + a$ (with the creation and annihilation operators $a^\dagger$ and a of the oscillator) onto the subspace of the ground state and the first excitation with basis $\{|0\rangle, |1\rangle\}$ via $a^\dagger a = \frac{1}{2}(\sigma^z + 1)$ and $a^\dagger + a = \sigma^x$ (with the usual 2×2 Pauli matrices), we will now include the third state $|3\rangle$ in the basis and project

$$a^\dagger a = \tau^z, \text{ and } a^\dagger + a = \tau^x, \tag{5.2}$$

with the matrices

$$\tau^z = \begin{pmatrix} 0 & 0 & 0 \\ 0 & 1 & 0 \\ 0 & 0 & 2 - \chi_\mathrm{r} \end{pmatrix}, \text{ and } \tau^x = \begin{pmatrix} 0 & 1 & 0 \\ 1 & 0 & \sqrt{2} \\ 0 & \sqrt{2} & 0 \end{pmatrix} \tag{5.3}$$

in the basis $\{|0\rangle, |1\rangle, |2\rangle\}$. We introduced $\chi_\mathrm{r} \in (0, 1)$ to account for the anharmonicity: We showed through perturbation theory in equation (2.21) that if the energy difference between ground and first excited state is ϵ, then the energy difference between first and second excited state is slightly smaller and can be expressed by $(1 - \chi_\mathrm{r})\epsilon = \epsilon - \chi$ with the anharmonicity $\chi = \chi_\mathrm{r}\epsilon$; this is pictured in figure 5.1.

Let us study a system of two transmons. The Hamiltonian just containing the energies of the transmons reads

$$H_0^\tau = \epsilon\tau_1^z + \epsilon\tau_2^z. \tag{5.4}$$

The state $|11\rangle$ has a higher energy E_{11} than the states $|20\rangle$ or $|02\rangle$ with energy E_{20}. For this reason we have to check that this is not an issue, i. e., that this does not allow for unwanted transitions if we include perturbations to this Hamiltonian. Our often encountered σ^x-type interaction would—in its generalized form with the new τ^x operators—play the role of such a perturbation. With the coupling energy g^x, we intro-

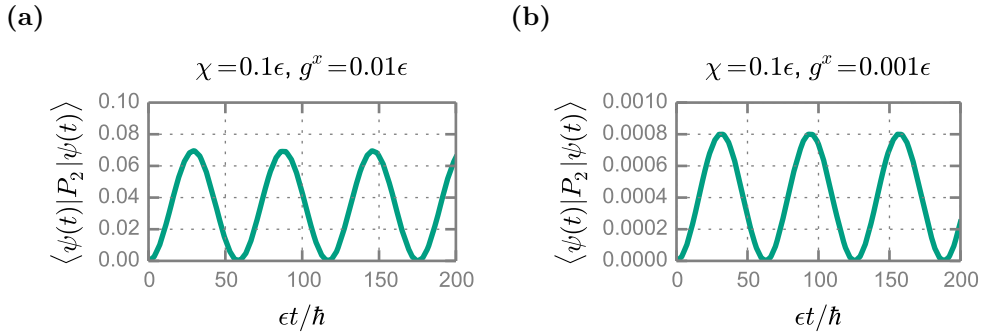

Figure 5.2: A system of two degenerate transmons generalized to three level systems, where the energy splitting of the first two levels is labeled ϵ. The transmons are coupled by the τ^x operators with coupling energy g^x. This is described by the Hamiltonian in equation (5.7). Plotted is the expectation value for a state $|\psi(t)\rangle$ having a transmon in its second excited state over time, with the initial state $|\psi(0)\rangle = |11\rangle$. In **(a)** the fraction of coupling energy over anharmonicity is $\frac{g^x}{\chi} = \frac{1}{10}$ and in **(b)** it is $\frac{g^x}{\chi} = \frac{1}{100}$. We can see how the estimated value of $8(\frac{g^x}{\chi})^2$ for the expectation value resulting from perturbation theory is in good agreement with the maximum values in the plots.

duce the interaction Hamiltonian

$$H_1^\tau = g^x \tau_1^x \tau_2^x. \tag{5.5}$$

In first order perturbation theory, the corrections to the state $|11\rangle$ would be of the order

$$\frac{\langle 20|H_1^\tau|11\rangle}{E_{11} - E_{20}} = \sqrt{2}\frac{g^x}{\chi}. \tag{5.6}$$

We can therefore see, that the anharmonicity $\chi = \chi_r\epsilon$ protects from unwanted transitions, as long as it is large compared to the coupling energy.

Let us study this further through numerical simulation. We take the full Hamiltonian

$$H_2^\tau = \epsilon\tau_1^z + \epsilon\tau_2^z + g^x\tau_1^x\tau_2^x \tag{5.7}$$

and look at the time evolution of a state $|\psi(t)\rangle$, where we start in the initial state $|\psi(0)\rangle = |11\rangle$. We introduce the projector P_2, which is the sum of the projectors on every state with roughly the same energy as $|11\rangle$, and with one transmon being in its third level:

$$P_2 = |20\rangle\langle 20| + |02\rangle\langle 02|. \tag{5.8}$$

We then simulate how the expectation value $\langle\psi(t)|P_2|\psi(t)\rangle$ evolves over time. From equation (5.6), since we have two contributions of this form, we can estimate that the expectation value of the projector should be of order $(2 \cdot \sqrt{2}\frac{g^x}{\chi})^2 = 8(\frac{g^x}{\chi})^2$. The results of the simulation in figure 5.2 show very good agreement to this estimate. Typical values for the anharmonicity are $\chi \approx \frac{\epsilon}{10}$, such that we can operate within a limit, where the coupling energy is much smaller than the anharmonicity; we want the coupling in our

emulator to be very small anyhow, as sections 2.4.2 and 3.1.2 demand this limit.

Unfortunately, the problem becomes worse if we generalize further by increasing the number of transmons to $n > 2$. We now obtain the Hamiltonian

$$H_n^\tau = \sum_{j=1}^{n} \epsilon \tau_j^z + g^x \sum_{j=1}^{n-1} \tau_j^x \tau_{j+1}^x, \tag{5.9}$$

and define the states

$$|i\rangle = |111\ldots\rangle, \text{ and } |f\rangle = \frac{1}{\sqrt{2(n-1)}}(|201\ldots\rangle + |021\ldots\rangle + |120\ldots\rangle + |102\ldots\rangle + \ldots). \tag{5.10}$$

This leads to the matrix element

$$\langle f|H_n^\tau|i\rangle = 2\sqrt{n-1}g^x, \tag{5.11}$$

which means that the coupling strength gets effectively enhanced by a factor $\sqrt{2(n-1)}$. Hence, for increasing n, the effective coupling energy will ultimately exceed the anharmonicity and the anharmonicity will not protect from transitions anymore. This would eventually limit our options regarding the scaling of an emulator to a large number of transmons. But we need to check first, whether or not there are additional effects, that avoid this problem.

For this, we study the presence of noise on the third level, because in reality, the third level is more susceptible to noise than the first two levels. We do this by introducing the operator

$$X = \begin{pmatrix} 0 & 0 & 0 \\ 0 & 0 & 0 \\ 0 & 0 & 1 \end{pmatrix}, \tag{5.12}$$

and then include dephasing terms in the Von Neumann equation for the density matrix ρ, leading to the Lindblad master equation

$$\dot{\rho} = \frac{1}{\mathrm{i}\hbar}[H_n^\tau, \rho] + \Gamma\big(X\rho X^\dagger - \frac{1}{2}(\rho X^\dagger X + X^\dagger X\rho)\big), \tag{5.13}$$

with the dephasing rate Γ of the third energy level. Restricting ourselves to the subspace with basis $\{|i\rangle, |f\rangle\}$, we find the matrix element

$$\langle f|\dot{\rho}|i\rangle = \frac{1}{\mathrm{i}\hbar} 2g^x\sqrt{n-1}(\langle i|\rho|i\rangle - \langle f|\rho|f\rangle) - \frac{1}{\mathrm{i}\hbar}\frac{\chi}{2}\langle f|\rho|i\rangle - \frac{\Gamma}{2}\langle f|\rho|i\rangle. \tag{5.14}$$

We can now read from this equation, that the term $-\frac{\Gamma}{2}\langle f|\rho|i\rangle$ suppresses excitations of a third level by lowering the transition rate of the problematic transition from $|i\rangle$ to $|f\rangle$. We can however also see that it lacks a scaling factor $\sqrt{n-1}$ and stays constant for an increasing system size. Hence, this mechanism gives additional protection to the one

from the anharmonicity and enables us to emulate larger systems, yet it still does not give the opportunity to scale the emulator up infinitely.

Unfortunately, further approaches of including noise on the third level gave similar results. We have to conduct more intense studying of this issue to completely answer the question how far our emulator design can be scaled up in principle. The investigation of additional effects to protect from undesired transitions will follow, possibly supported by numerical simulations to quickly obtain impressions how certain approaches impact our system.

5.3 Gaining Confidence trough Measurement

We suggest an additional approach to purely theoretical methods to understand how large the errors in an emulator are: By measuring local operators, one could examine properties of the emulated system which were known beforehand.

To explain this in more detail, let us refer to our emulator of the one-dimensional Fermi-Hubbard model. Section 4.2 showed that we can in principle measure the occupation of any of the fermionic states. If we resort to the Hamiltonian

$$H_{\mathrm{FH}} = U \sum_{j=1}^{n} c_{j,\uparrow}^{\dagger} c_{j,\uparrow} c_{j,\downarrow}^{\dagger} c_{j,\downarrow} - t \sum_{j=1}^{n-1} \sum_{s=\uparrow,\downarrow} (c_{j,s}^{\dagger} c_{j+1,s} + c_{j+1,s}^{\dagger} c_{j,s}) \tag{5.15}$$

of the Fermi-Hubbard model (from equation (2.27)), we can identify a variety of different properties of this system: For example it is symmetrical regarding the interchanging of spin-up and spin-down states. In the emulator we should therefore measure equivalent results on either of the qubit chains that represent the spin-up or the spin-down states. Also the number of total excitations of both spin-up and spin down-states are preserved, hence the total excitations in each of the transmon chains should be preserved as well. For a sufficiently large number of sites n, neglecting boundary effects, we find a translational symmetry along the sites which should equally be present in the emulator. If one would initialize excitations in only one qubit chain, the σ^z interactions to the other chain would only apply a constant shift to the qubit energies. This means that one would effectively obtain a Heisenberg XX-chain of qubits with equal excitation energy coupled by their σ^x operators; this model has an analytic solution that could be compared to the emulation results. Another option would be to emulate system sizes that are accessible through numerical simulation, such that emulation results could be compared to the simulation.

We explained how we could perform measurements on an emulator, which could then be compared to known quantities. Consequently, we might be able to gain confidence in the results the emulator produces, or to reveal possible limitations of the emulation.

This procedure could be seen as a calibration scheme and could in general also be performed on other emulators apart from one for the Fermi-Hubbard model. It could furthermore play an important role to support the theoretical approaches on quantifying

errors, as it could supply data for comparison to these theoretical approaches; eventually helping to understand under which circumstances the results of a quantum emulation could be trusted.

With this insight, we close this chapter on error discussion. We have revealed interesting questions, but these will be addressed in future work; it is now a suitable moment to conclude this thesis.

Chapter 6

Summary and Outlook

After the introduction, chapter 2 started by establishing the elementary concepts this thesis dealt with. Section 2.1 explained the concept of quantum emulation and the motivation behind it. It also stated four criteria that a quantum emulator needs to satisfy. These criteria will be addressed explicitly in a moment. Section 2.2 presented the technology of superconducting circuits, which was used to conceptualize the quantum emulator in this thesis. It started by giving an overview how quantum circuits are treated to obtain their quantum mechanics in 2.2.1 and continued by explaining the tunable transmon qubit in 2.3 as the fundamental element in our emulator. This was followed by section 2.4, where the Jordan-Wigner transformation was used to show the equivalence of the one-dimensional Fermi-Hubbard model to a qubit system where each qubit as a two level system represents a distinct fermionic state that can be occupied or non-occupied. We obtained how the on-site interaction energy in the fermionic model is equivalent to a σ^z coupling of the qubits, and showed that σ^x-type interaction in the qubit system gives the hopping term of the Fermi-Hubbard model; hence, we obtained an emulator for this fermionic model.

We then showed how to construct this emulator in chapter 3. We derived in section 3.1, that—using transmons as qubits—we can achieve the σ^x-type interaction either through coupling via inductances (see section 3.1.1) or via capacitances (see section 3.1.2), where we also gave expressions for the coupling energies depending on the circuit elements. This was concluded by stating why the capacitative coupling is favorable in experiment. We continued in 3.2 by deriving the more subtle method of coupling two transmons by a mutual inductance formed by their intrinsic inductances, which results in a σ^z-type interaction between the transmons. We first showed how to treat a mutual inductance in the context of superconducting circuits in 3.2.1, and then continued with the derivation of the coupling of two transmons by a mutual inductance in 3.2.2, and again obtained an expression for the coupling strength depending on the circuit elements. Lastly, section 3.3 summarized the findings up to that point and provided the full circuit for the emulator of the Fermi-Hubbard model in section 3.3.1 as a major achievement of this thesis. We further discussed the tunability of the circuit

in 3.3.2 and finished in 3.3.3 with a brief discussion regarding the realization—possibly in the near future—of the presented circuits in experiment.

Chapter 4 continued with the initialization and readout process for the emulator. Naturally, we started by explaining in detail in section 4.1, how the standard approach to initialize a qubit from its ground into its excited state functions. We then presented a circuit for a potential readout scheme based on the mechanics of coupling the transmon by a mutual inductance from section 3.2.2 as an additional method to the standard readout procedure. An investigation how to treat multiple transmons coupled among themselves followed in 4.3, in order to give a complete scheme, how we intend to perform the initialization and readout in our emulator.

Finally, chapter 5 gave a brief discussion on errors regarding the general error sources of temperature and disorder in section 5.1 and the possible excitations of the second excited state in a transmon in section 5.2, which is a specific problem for our emulator design. This was followed by a method to gain confidence in the emulation results by measuring quantities that are known beforehand in 5.3.

To finish this summary, let us examine whether or not our proposed quantum emulator for the one-dimensional Fermi-Hubbard model matches the four criteria for a quantum emulator from section 2.1.

The first criterion of relevance is matched, since the Fermi-Hubbard model is of course an interesting model worth studying. Section 3.3.2 showed that we have the possibility of tuning the parameters of the emulator and chapter 4 showed the options for initialization and readout; therefore we fulfill the second requirement of controllability. The forth criterion of efficiency is also satisfied, as there are properties of the Fermi-Hubbard model that cannot be attained through analytic calculation or numerical simulation on a classical computer yet.

The question whether we can trust the results of the emulator is however difficult to answer at this point, therefore the third criterion of reliability is a delicate matter. Chapter 5 showed that further studying needs to be done, regarding the excitations of the third level of transmons (see section 5.2), the effects of temperature in the system, and the more general question how to predict the errors on the emulation results depending on the deviations of the emulator from the ideal system (see section 5.1). On the other hand section 5.3 showed that the realization of an emulator could supply data to support these theoretical questions, such that it is certainly worth the effort to try to build an emulator in experiment.

In the end, these experimental and theoretical challenges posed by this thesis could be a guidance for interesting work to follow in near future.

Bibliography

[1] P. W. Shor: *Polynomial-Time Algorithms for Prime Factorization and Discrete Logarithms on a Quantum Computer.* SIAM J.Sci.Statist.Comput. **26**, 1484 (1997).

[2] L. M. K. Vandersypen, M. Steffen, G. Breyta, C. S. Yannoni, M. H. Sherwood and I. L. Chuang: *Experimental realization of Shor's quantum factoring algorithm using nuclear magnetic resonance.* Nature **414**, 883-887 (2001).

[3] S. Lloyd: *Universal Quantum Simulators.* Science **273**, 1073 (1996).

[4] R. P. Feynman: *Simulating physics with computers.* International Journal of Theoretical Physics **21**, 467 (1982).

[5] A. G. Fowler, M. Mariantoni, J. M. Martinis and A. N. Cleland: *Surface codes: Towards practical large-scale quantum computation.* Phys. Rev. A **86**, 032324 (2012).

[6] T. Esslinger: *Fermi-Hubbard Physics with Atoms in an Optical Lattice.* Annual Review of Condensed Matter Physics **1**, 129 (2010).

[7] N. Goldman: *Mott-insulator transition for ultracold fermions in two-dimensional optical lattices.* Phys. Rev. A **77**, 053406 (2008).

[8] G. Wendin and V. S. Shumeiko: *Superconducting Quantum Circuits, Qubits and Computing.* arXiv:cond-mat/0508729v1 (2005).

[9] J. Clarke and F. K. Wilhelm: *Superconducting quantum bits.* Nature **453**, 1031 (2008).

[10] M. H. Devoret, A. Wallraff and J. M. Martinis: *Superconducting Qubits: A Short Review.* arXiv:cond-mat/0411174 (2004).

[11] J. Koch, T. M. Yu, J. Gambetta, A. A. Houck, D. I. Schuster, J. Majer, A. Blais, M. H. Devoret, S. M. Girvin and R. J. Schoelkopf: *Charge-insensitive qubit design derived from the Cooper pair box.* Phys. Rev. A **76**, 042319 (2007).

[12] H. Paik, D. I. Schuster, L. S. Bishop, G. Kirchmair, G. Catelani, A. P. Sears, B. R. Johnson, M. J. Reagor, L. Frunzio, L. Glazman, S. M.

Girvin, M. H. Devoret and R. J. Schoelkopf: *Observation of high coherence in Josephson junction qubits measured in a three-dimensional circuit QED architecture.* arXiv:1105.4652v4 (2011).

[13] C. Rigetti, J. M. Gambetta, S. Poletto, B. L. T. Plourde, J. M. Chow, A. D. Córcoles, J. A. Smolin, S. T. Merkel, J. R. Rozen, G. A. Keefe, M. B. Rothwell, M. B. Ketchen and M. Steffen: *Superconducting qubit in waveguide cavity with coherence time approaching 0.1ms.* Phys. Rev. B **86**, 100506(R) (2012).

[14] P. Hauke, F. M. Cucchietti, L. Tagliacozzo1, I. Deutsch and M. Lewenstein: *Can one trust quantum simulators?* Rep. Prog. Phys. **75**, 082401 (2012).

[15] P. Jordan and E. Wigner: *Über das Paulische Äquivalenzverbot.* Zeitschrift für Physik **47**, No. 9 pp. 631-651 (1928).

[16] E. H. Lieb and F.-Y. Wu: *Absence of Mott Transition in an Exact Solution of the Short-Range, One-Band Model in One Dimension.* Phys. Rev. Lett. **21**, 192 (1968).

[17] E. H. Lieb and F.-Y. Wu: *The one-dimensional Hubbard model: A reminiscence.* arXiv:cond-mat/0207529 (2002).

[18] F. H. L. Essler, H. Frahm, F. Göhmann, A. Klümper and V. E. Korepin: *The One-Dimensional Hubbard Model.* Cambridge University Press (2005).

[19] G. Y. Hu and R. F. O'Connell: *Analytical inversion of symmetric tridiagonal matrices.* Phys. A: Math. Gen. **29**, 1511 (1996).

[20] R. S. Elliott: *Electromagnetics.* IEEE Press and Oxford University Press, 1999.

[21] C. Kittel: *Introduction to Solid State Physics.* 5th edition. p. 367. New York: John Wiley & Sons, Inc (1976).

Danksagungen

Ich bedanke mich bei Gerd Schön dafür, meine Masterarbeit am Institut für Theoretische Festkörperphysik abgelegt haben zu dürfen und für die Bemühungen mir ein weiteres Arbeiten an diesem Institut zu ermöglichen, außerdem bei Alexey Ustinov für das zur Verfügung stellen als Korreferent.

Ebenso bedanke ich mich bei meinen Kollegen für die schöne und lockere Arbeitsatmosphäre sowie die vielen lustigen Momente – auch außerhalb der Arbeitszeit.

Hervorheben will ich die Betreuung durch Michael Marthaler, welcher sich auch in stressigen Situationen immer versucht die Zeit für ergiebige Diskussionen und nötige Hilfestellungen zu nehmen, wofür ich mich besonders bedanke.

Mir gefällt die Arbeit an diesem Institut sehr; nicht ohne Grund kam ich seit der Teilnahme an einem Hauptseminar dieser Arbeitsgruppe in meinem fünften Semester – und damit seit der halben Zeit meines Studiums – in gewissen Abständen für meine Bachelorarbeit und nun auch für meine Masterarbeit gerne wieder. Und nicht ohne Grund entschied ich mich dafür eine Promotion an diesem Institut anzugehen.

Ein spezieller Dank geht an meinen Bruder, der sich trotz der zahlreichen schönen Möglichkeiten ein Wochenende zu verbringen dazu bereit erklärte, diese Arbeit Korrektur zu lesen und mir viele wertvolle Verbesserungsvorschläge zukommen ließ.